Journal of Medicinal Chemistry

pubs.acs.org/jmc Article

Structure–Activity Relationship Study of Dexrazoxane Analogues Reveals ICRF-193 as the Most Potent Bisdioxopiperazine against Anthracycline Toxicity to Cardiomyocytes Due to Its Strong Topoisomerase IIβ Interactions

Anna Jirkovská,* Galina Karabanovich, Jan Kubeš, Veronika Skalická, Iuliia Melnikova, Jan Korábečný, Tomáš Kučera, Eduard Jirkovský, Lucie Nováková, Hana Bavlovič Piskáčková, Josef Škoda, Martin Štěrba, Caroline A. Austin, Tomáš Šimůnek, and Jaroslav Roh*

Cite This: *J. Med. Chem.* 2021, 64, 3997–4019 Read Online

ACCESS | Metrics & More | Article Recommendations | Supporting Information

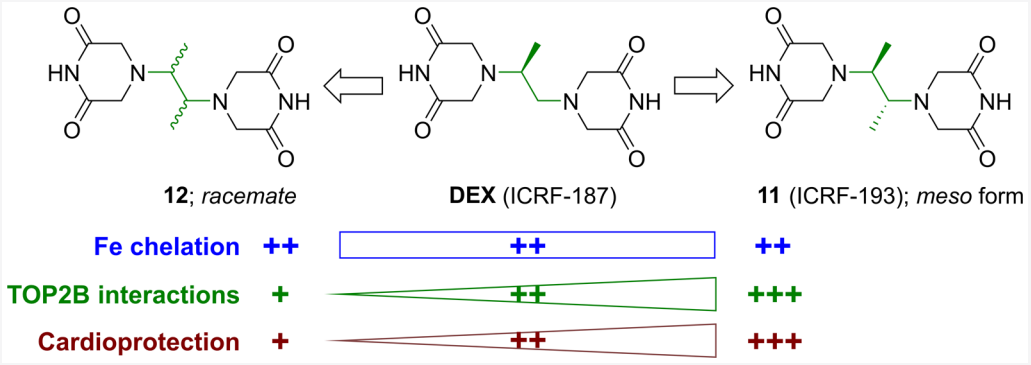

ABSTRACT: Cardioprotective activity of dexrazoxane (ICRF-187), the only clinically approved drug against anthracycline-induced cardiotoxicity, has traditionally been attributed to its iron-chelating metabolite. However, recent experimental evidence suggested that the inhibition and/or depletion of topoisomerase IIβ (TOP2B) by dexrazoxane could be cardioprotective. Hence, we evaluated a series of dexrazoxane analogues and found that their cardioprotective activity strongly correlated with their interaction with TOP2B in cardiomyocytes, but was independent of their iron chelation ability. Very tight structure–activity relationships were demonstrated on stereoisomeric forms of 4,4′-(butane-2,3-diyl)bis(piperazine-2,6-dione). In contrast to its rac-form **12**, meso-derivative **11** (ICRF-193) showed a favorable binding mode to topoisomerase II *in silico*, inhibited and depleted TOP2B in cardiomyocytes more efficiently than dexrazoxane, and showed the highest cardioprotective efficiency. Importantly, the observed ICRF-193 cardioprotection did not interfere with the antiproliferative activity of anthracycline. Hence, this study identifies ICRF-193 as the new lead compound in the development of efficient cardioprotective agents.

INTRODUCTION

The bisdioxopiperazines have been originally discovered as drug candidates accidentally while attempting to develop less polar and thus cell-permeable derivatives of the metal chelator ethylenediaminetetraacetic acid (EDTA) as antineoplastic agents.[1] Notable antiproliferative effects were observed in several members of this class[2] and further early preclinical studies performed with ICRF-159 (razoxane, a racemic mixture of dexrazoxane and levrazoxane, Figure 1) demonstrated high antitumor activity and antimetastatic effects when combined with established anticancer drugs, including anthracyclines (ANT).[3,4] The same effect was found in its more soluble enantiomer dexrazoxane (ICRF-187, DEX) or another bisdioxopiperazine ICRF-154.[5] Further investigations disproved the validity of the metal chelation hypothesis for their anticancer effect and established catalytic inhibition of topoisomerase II (TOP2) as the key mechanism.[6,7] In-depth mechanistic studies generally supported the catalytic mode of TOP2 inhibition,[8−11] despite some studies that offered an alternative perspective.[12,13] DEX and other bisdioxopiperazines do not bind directly to the adenosine 5′-triphosphate (ATP)-binding pocket of TOP2 but instead they bind to the so-called DEX binding site where they bridge and stabilize a transient

Received: December 14, 2020
Published: March 22, 2021

Downloaded via BUTLER UNIV on May 15, 2021 at 21:09:55 (UTC).
See https://pubs.acs.org/sharingguidelines for options on how to legitimately share published articles.

ACS Publications © 2021 American Chemical Society

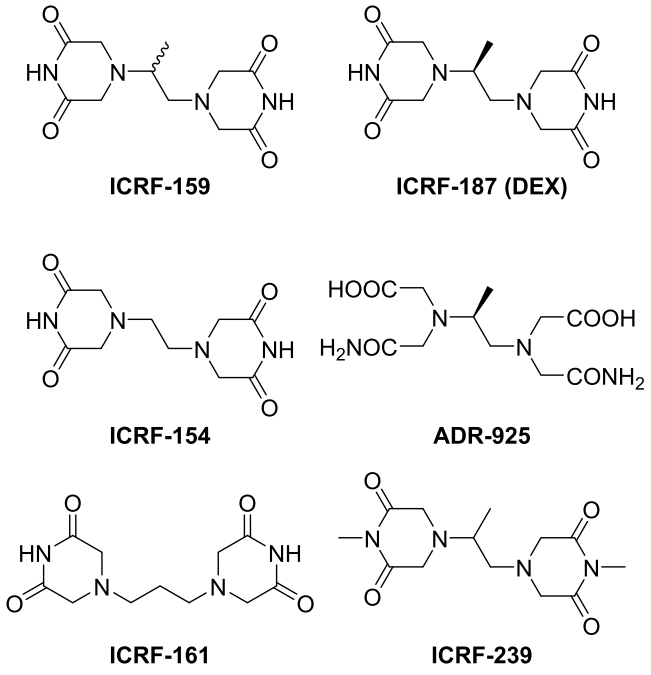

Figure 1. Bisdioxopiperazine ICRF-187 (DEX), its metabolite ADR-925 and several DEX analogues previously studied for protection against anthracycline cardiotoxicity.

dimer interface between the two ATPase protomers of TOP2.[14] This site was confirmed by studies using mutated enzymes and later by the crystallization experiments. Based on the mutations of different amino acids, some studies also suggested other binding sites, mainly in the core domain of the protein.[15,16] Nevertheless, the crystal structure of the core part of TOP2 with bound DEX or other bisdioxopiperazine has not been described yet.

Over decades, the structure−activity relationships (SAR) of bisdioxopiperazines have been well characterized with respect to both topoisomerase II (TOP2) inhibition and anticancer effects.[17−20] However, with the exception of sobuzoxane,[21] none of these agents has progressed to advanced clinical evaluation or routine clinical use. Even the most potent analogue of this class, ICRF-193, has not progressed beyond its use as an experimental tool and model TOP2 catalytic inhibitor.

Interestingly, the cardioprotective effects of bisdioxopiperazine compounds were recognized later, and in contrast to the anticancer effects, it has been successfully translated into clinical use. In cardioprotective settings, DEX has dominated as its markedly increased solubility allowed intravenous administration.[22] So far, DEX has been the only drug that unambiguously protected the heart against chronic type of ANT cardiotoxicity in different animal models[23] and has been approved for this indication in clinical practice.[24] Despite some concerns, meta-analyses of all randomized controlled trials confirmed that significant cardioprotection is achieved without interference with anticancer effects of ANTs.[24,25]

The mechanism(s) of cardioprotective activity of DEX remains controversial. DEX has been found to undergo metabolization to EDTA-like ring-opened chelating agent ADR-925 (Figure 1).[26,27] ANTs and particularly their iron complexes are redox-active and can form highly toxic reactive oxygen species (ROS). It has been widely accepted that DEX

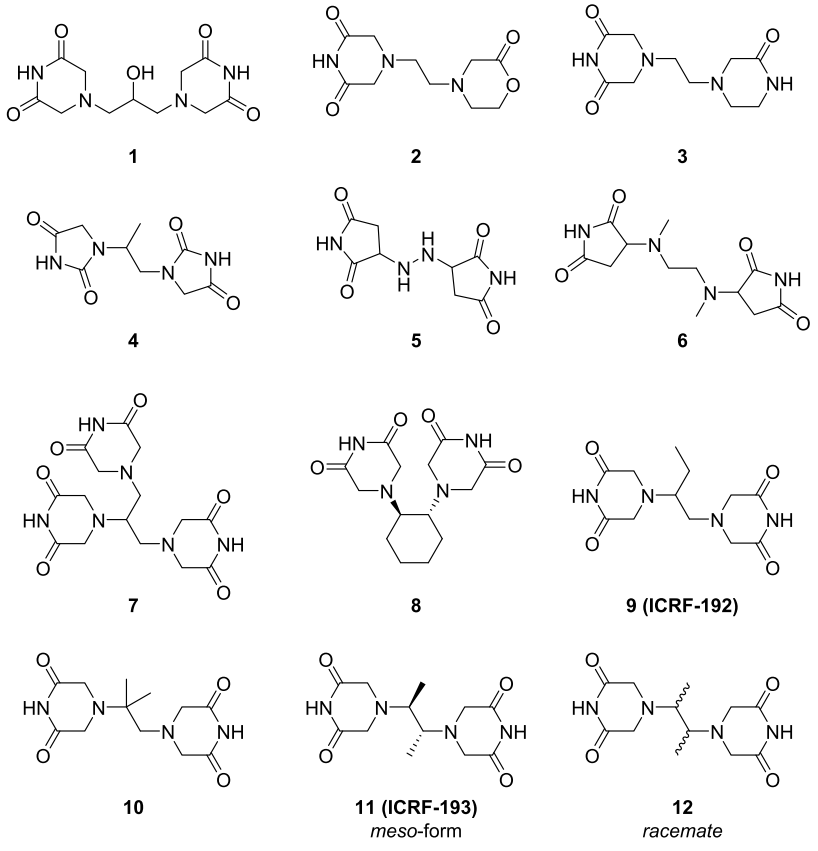

Figure 2. Structures of DEX analogues **1**−**12** that were prepared and studied in this work.

https://doi.org/10.1021/acs.jmedchem.0c02157
J. Med. Chem. 2021, 64, 3997−4019

Scheme 1. Synthesis of 4,4′-(2-Hydroxypropane-1,3-diyl)bis(piperazine-2,6-dione) (1), 4-(2-(2-Oxomorpholin-4-yl)ethyl)piperazine-2,6-dione (2), and 4-(2-(3-Oxopiperazin-1-yl)ethyl)piperazine-2,6-dione (3)[a]

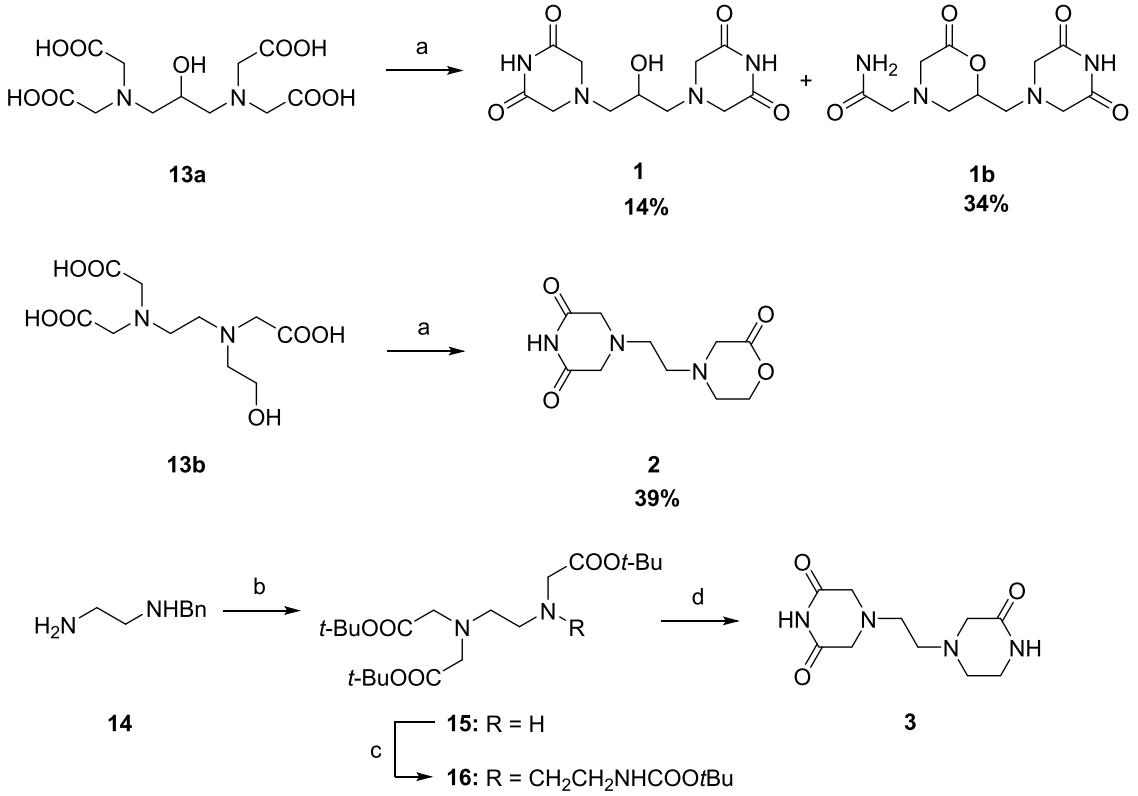

[a]Reagents and conditions: (a) 1. $HCONH_2$, vacuum (30 mbar), 110 °C, 1.5 h; 2. 155 °C, 5 h, Ar; (b) 1. $BrCH_2COOtBu$, K_2CO_3, tetrahydrofuran (THF), H_2O, reflux, 4 h, 91%; 2. H_2, Pd/C, MeOH, room temperature (rt), 24 h, 94%; (c) $Br(CH_2)_2NHCOOtBu$, K_2CO_3, CH_3CN, reflux, 48 h, 55%; (d) 1. 36% aq. HCl, 90 °C, 2 h; 2. $HCONH_2$, vacuum (30 mbar), 110 °C, 1 h; 3. $HCONH_2$, 160 °C, 5 h, Ar, 24%.

prevents ANT-induced oxidative injury *via* iron chelation. In this regard, the lipophilicity of DEX ensures its penetration into the cardiac cells, where, upon the hydrolytic opening, the metabolite chelates iron ions and displaces them from the ANT complexes. However, several studies showed that other effective iron chelators[23,28] or DEX analogues with preserved iron-chelating properties[29,30] were not able to protect the heart from ANT cardiotoxicity. Furthermore, an accumulating body of evidence implies that an alternative mechanism may be important for cardioprotection.[31−33] In particular, interaction with topoisomerase IIβ (TOP2B), which is the predominant TOP2 isoform in cardiomyocytes,[34,35] has been attributed to the cardioprotective effects of DEX against ANT cardiotoxicity. The latter hypothesis has been supported by a nonpharmacological approach where cardiac-specific TOP2B knock-out effectively protected mice from ANT cardiotoxicity.[36]

In sharp contrast to anticancer effects, SAR studies of bisdioxopiperazines with respect to cardioprotection have been scarce and this matter remains poorly understood. Besides DEX, only demethylated DEX analogue ICRF-154,[37] its prodrug sobuzoxane (MST-16), and morpholine prodrug of ICRF-159 probimane[21,31,38] showed a clear cardioprotective potential. Other bisdioxopiperazine derivatives tested so far, including close DEX homologues ICRF-161[29] and ICRF-192,[37] amide analogue MK-15,[30] or *N*,*N*′-dimethyl analogue ICRF-239,[39] showed negative results.

Hence, the aim of this work was to design, synthesize, and examine the SAR in the series of several structural types of DEX analogues with respect to cardioprotection. We focused on their interaction with both TOP2 isoforms and the iron-chelating activities of their hydrolysis products to provide mechanistic explanations of the observed effects. The first two DEX analogues **1** and **2** were designed to produce iron-chelating metabolites, as they are the closed-ring derivatives of known iron chelators 1,3-diamino-2-hydroxypropane-*N*,*N*,*N*′,*N*′-tetraacetic acid and *N*-(2-hydroxyethyl)-ethylenediamine-*N*,*N*′,*N*′-triacetic acid, respectively (Figure 2). DEX analogue **1** is a close analogue of ICRF-161, while **2** and particularly **3** are analogues of ICRF-154. DEX analogue **3** differs from ICRF-154 only in one oxo group; it carries one amide group instead of an imide group. Five-membered ring analogues **4**−**6** were designed to mimic the original 3,5-dioxopiperazine cycles in DEX. Especially in analogues **5** and **6**, both imides and two basic amines as in the original DEX molecule are preserved and in the latter case also the distance of the two imide end groups is close to that of DEX. The analogues **7**−**12** were designed to closely mimic the structure of DEX; the changes were made merely in the linker between two 3,5-dioxopiperazine moieties. Analogue **7** carries one more 3,5-dioxopiperazine connected to the linker of the original DEX. Analogue **8** was derived from a known chelator *trans*-1,2-cyclohexanediamine-*N*,*N*,*N*′,*N*′-tetraacetic acid; thus, its linker between both 3,5-dioxopiperazines is a part of cyclohexyl ring. Analogues **9**−**12** are the simplest homologues of DEX, with merely one inserted methyl group. Since both enantiomers, DEX (ICRF-187) and levrazoxane (LEV, ICRF-186), are similarly effective TOP2 inhibitors[7] and also similarly effective

https://doi.org/10.1021/acs.jmedchem.0c02157
J. Med. Chem. 2021, 64, 3997−4019

Scheme 2. Synthesis of 1,1′-(Propane-1,2-diyl)bis(imidazolidine-2,4-dione) (4), 3,3′-(Hydrazine-1,2-diyl)bis(pyrrolidine-2,5-dione) (5), and *N*,*N*′-bis(2,5-Dioxopyrrolidin-3-yl)-*N*,*N*′-dimethylethylenediamine (6)[a]

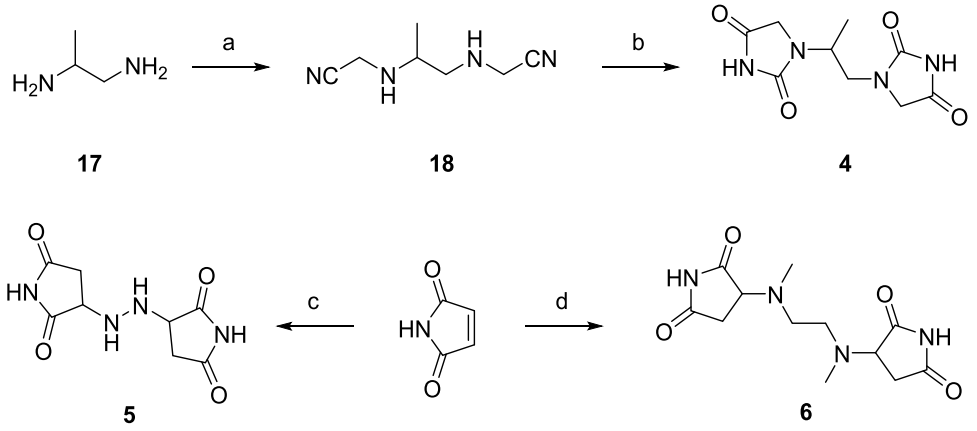

[a]Reagents and conditions: (a) $HOCH_2CN$, H_2O, rt, 12 h, 77%; (b) 1. NaOH, H_2O, 80 °C, 3 h; 2. KOCN, H_2O, reflux, 1 h, 5%; (c) $N_2H_4.H_2O$, EtOH, rt, 48 h, 69%; (d) *N*,*N*′-dimethylethylenediamine (DMEDA), THF, rt, 10 h, 38%.

Scheme 3. Unwanted Rearrangements Observed during the Addition of Diamines to Maleimide

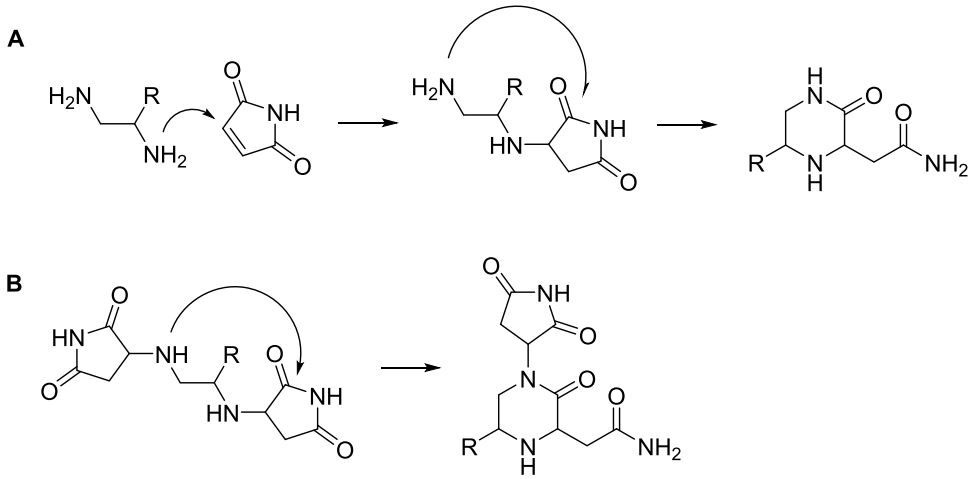

against ANT-induced cardiotoxicity *in vivo*,[40] most analogues were prepared and studied as the racemates (**4**, **8**, **9** and **12**) or the mixtures of all diastereoisomers (**5** and **6**, Figure 2).

RESULTS

Chemistry. 4,4′-(2-Hydroxypropane-1,3-diyl)bis-(piperazine-2,6-dione) (**1**) and 4-(2-(2-oxomorpholin-4-yl)-ethyl)piperazine-2,6-dione (**2**) were prepared from known chelators 1,3-diamino-2-hydroxypropane-*N*,*N*,*N*′,*N*′-tetraacetic acid (**13a**) and *N*-(2-hydroxyethyl)ethylenediamine-*N*,*N*′,*N*′-triacetic acid (**13b**), respectively, using standard DEX synthesis consisted of heating in formamide under reduced pressure at 100−110 °C for 1−2 h, followed by heating under an argon atmosphere at 150−160 °C for 5 h.[41] However, the free hydroxy group in substrate **13a** facilitated the unwanted formation of lactone type product 2-(2-((3,5-dioxopiperazin-1-yl)methyl)-6-oxomorpholino)acetamide (**1b**) that further complicated the isolation and purification of target product **1**. Thus, the yield of DEX analogue **1** was only 14% (Scheme 1). The yield of DEX analogue **2** was 39% and was isolated using a standard workup; it crystallized upon evaporation of the excess formamide and addition of cold methanol.

Although 4-(2-(3-oxopiperazin-1-yl)ethyl)piperazine-2,6-dione (**3**) was the lactam analogue of compound **2**, a completely different procedure had to be used to successfully prepare it. Several attempts to use chelator **13b** as the starting material failed. Thus, the synthesis started from *N*-benzylethylenediamine (**14**) that was converted in two steps to tri(*tert*-butyl) 1,2-diaminoethane-*N*,*N*′,*N*′-triacetate (**15**).[39] The reaction of substrate **15** with *tert*-butyl (2-bromoethyl)-carbamate, followed by complete deprotection and cyclization in formamide, providing DEX analogue **3** in 11% overall yield (Scheme 1).

1,1′-(Propane-1,2-diyl)bis(imidazolidine-2,4-dione) (**4**) was prepared using a three-step procedure from 1,2-diaminopropane **17**. The first step consisted of the preparation of (propane-1,2-diyldiimino)diacetonitrile (**18**) using Strecker synthesis. The resulting dinitrile **18** was hydrolyzed to the corresponding diacetic acid, which upon the reaction with KOCN[42] gave DEX analogue **4** in 4% overall yield (Scheme 2).

The syntheses of succinimide-type DEX analogues **5** and **6** consisted of the addition of appropriate diamine to two molecules of maleimide (Scheme 2). There were two main problems with these reactions. The intermediates, which were

https://doi.org/10.1021/acs.jmedchem.0c02157
J. Med. Chem. 2021, 64, 3997−4019

Scheme 4. Six-Step Synthesis of 4,4′,4′′-(Propane-1,2,3-triyl)tris(piperazine-2,6-dione) (7)[a]

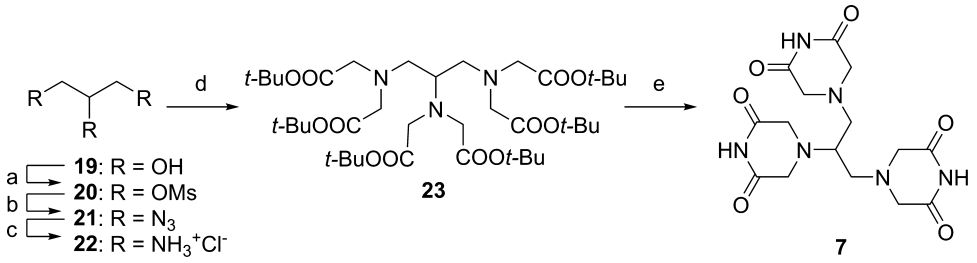

[a]Reagents and conditions: (a) MsCl, Et_3N, CH_3CN, rt, 48 h, 99%; (b) NaN_3, *N*,*N*-dimethylformamide (DMF), 85 °C, 5 h, 91%; (c) 1. $N_2H_4.H_2O$, Pd/C, EtOH, reflux, 12 h; 2. 36% aq. HCl, EtOH, 70%; (d) $BrCH_2COOtBu$, K_2CO_3, THF, H_2O, reflux, 25 h, 44%; (e) 1. 36% aq. HCl, H_2O, 90 °C, 4.5 h; 2. $HCONH_2$, vacuum (30 mbar), 115 °C, 1.5 h; 3. $HCONH_2$, 160 °C, 5 h, Ar, 40%.

Scheme 5. Syntheses of DEX Analogues 8−12[a]

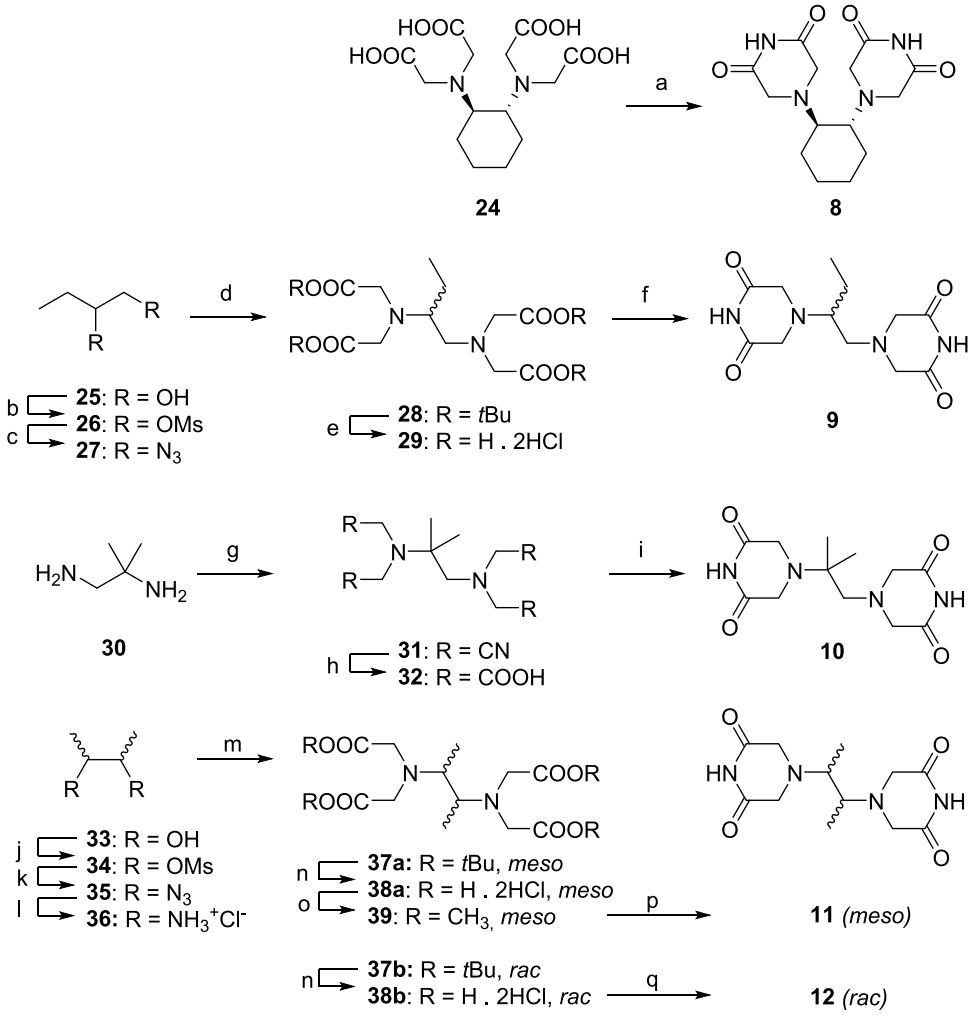

[a]Reagents and conditions: (a) 1. $HCONH_2$, vacuum (30 mbar), 110 °C, 1.5 h; 2. $HCONH_2$, 155 °C, 5 h, Ar, 57%; (b) MsCl, Et_3N, CH_2Cl_2, rt, 48 h, 76%; (c) NaN_3, DMF, 85 °C, 5 h, 60%; (d) 1. H_2, Pd/C, MeOH, 1 month; 2. $BrCH_2COOtBu$, K_2CO_3, THF, H_2O, reflux, 12 h, 29%; (e) 36% aq. HCl, 90 °C, 4 h, 97%; (f) 1. $HCONH_2$, vacuum (3 mbar), 110 °C, 1.5 h; 2. $HCONH_2$, 155 °C, 5 h, Ar, 44%; (g) CH_2O, H_2SO_4, NaCN, H_2O, 35 °C, 40 h, 19%; (h) $Ba(OH)_2.8H_2O$, H_2O, reflux, 24 h, 58%; (i) 1. $HCONH_2$, vacuum (30 mbar), 110 °C, 1.5 h; 2. $HCONH_2$, 155 °C, 5 h, Ar, 18%; (j) MsCl, Et_3N, CH_2Cl_2, rt, 2 h, 99%; (k) NaN_3, DMF, 85 °C, 6 h; (l) 1. H_2, Pd/C, MeOH, 1 month; 2. HCl (g), 38% over two steps; (m) $BrCH_2COOtBu$, K_2CO_3, THF, H_2O, reflux, 24 h, 76% (**37a**), 4% (**37b**); (n) 36% aq. HCl, H_2O, 85 °C, 3 h, 99%; (o) $SOCl_2$, MeOH, rt, 24 h, 91%; (p) $HCONH_2$, NaH, dioxane, Ar, rt, 24 h, 55%; (q) 1. $HCONH_2$, vacuum (30 mbar), 110 °C, 1.5 h; 2. $HCONH_2$, 150−160 °C, 5 h, Ar, 20%.

formed after the addition of a single amine group to one maleimide, tended to rearrange into lactam products (Scheme 3A). Moreover, when ethylenediamine or 1,2-diaminopropane were used, the final products quickly rearranged to the corresponding lactams (Scheme 3B). The former unwanted rearrangement can be reduced by the slow addition of diamine to the excess of maleimide. To prevent the latter type of rearrangement, we were forced to use *N*,*N*′-dimethylethylene-

https://doi.org/10.1021/acs.jmedchem.0c02157
J. Med. Chem. 2021, 64, 3997−4019

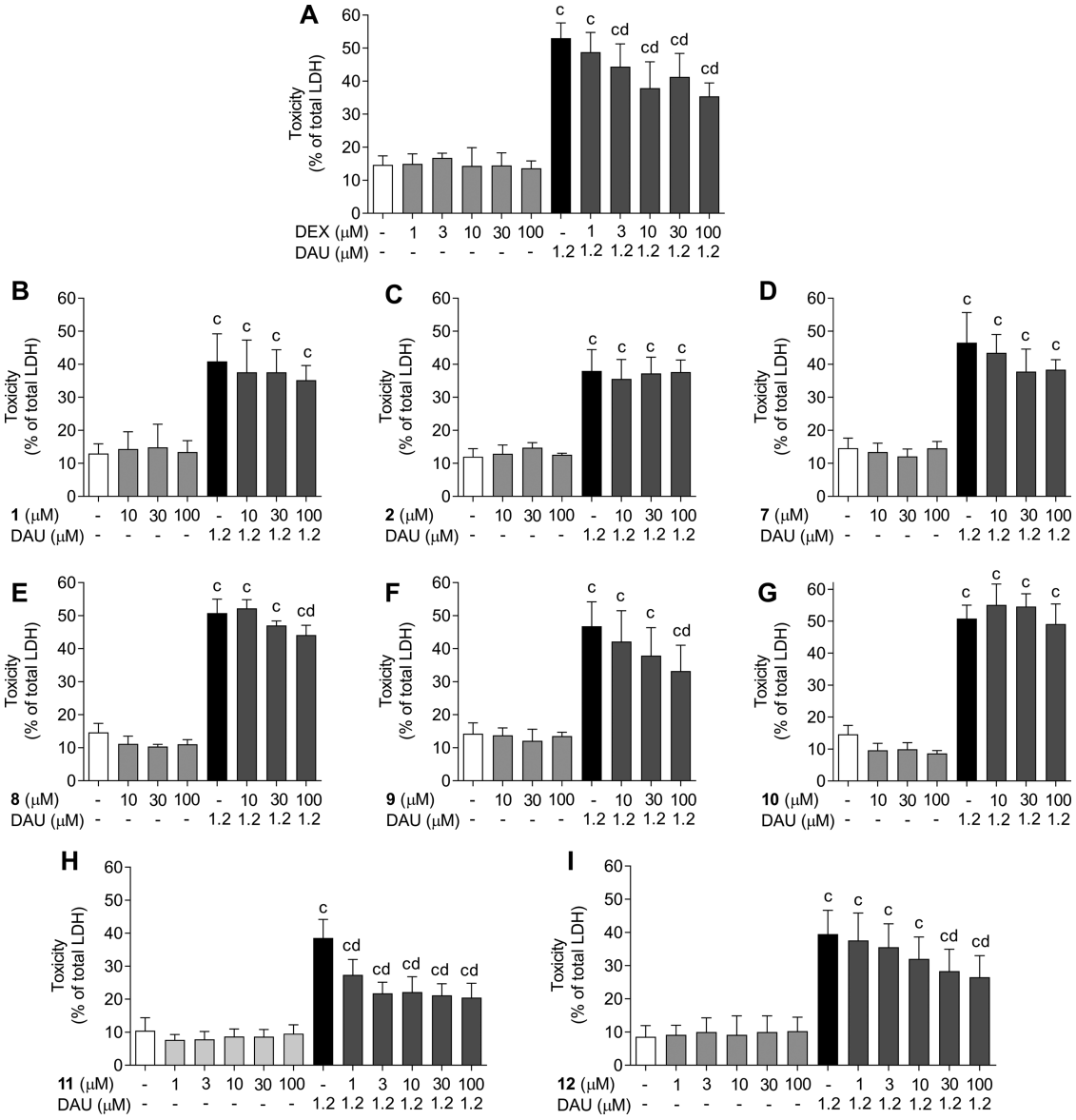

Figure 3. Toxicities of DEX and compounds **1**, **2**, **7**−**12**, and their protective effects on the DAU-induced cardiotoxicity in primary isolated rat cardiomyocytes. The data from four experiments are expressed as mean ± standard deviation (SD). Statistical significance was determined in GraphPad Prism 8 using the one-way analysis of variance (ANOVA) with the Holm−Sidak *post hoc* test and was accepted at $P \leq 0.05$: c, significant difference to control and d, significant difference to DAU.

diamine to obtain a stable tertiary amine-containing DEX analogue **6**.

4,4′,4′′-(Propane-1,2,3-triyl)tris(piperazine-2,6-dione) (**7**) was prepared using a six-step procedure starting from glycerol **19** (Scheme 4). First, glycerol was mesylated and then converted to 1,2,3-triazidopropane **21** by the reaction with sodium azide. 1,2,3-Triazidopropane **21** was reduced on Pd/C to propane-1,2,3-triamine trihydrochloride (**22**) according to the known method.[43] Its alkylation with *tert*-butyl bromoacetate yielded hexa(*tert*-butyl) 1,2,3-triaminopropane-*N*,*N*,*N*′,*N*′,*N*′′,*N*′′-hexaacetate (**23**). Hydrolysis of **23** followed by the final cyclization using a standard procedure in formamide resulted in the formation of final DEX analogue **7** in 11% overall yield.

The last step of the preparation of DEX analogues **8**−**11** was the cyclization of corresponding tetraacetic acids. Chelator *trans*-1,2-cyclohexanediamine-*N*,*N*,*N*′,*N*′-tetraacetic acid monohydrate **24** used for the synthesis of *trans*-4,4′-(cyclohexane-1,2-diyl)bis(piperazine-2,6-dione) (**8**) was commercially available. 1,2-Diaminobutane-*N*,*N*,*N*′,*N*′-tetraacetic acid dihydrochloride (**29**) used for the synthesis of 4,4′-(butane-1,2-diyl)bis(piperazine-2,6-dione) (**9**) was prepared from 1,2-butanediol (**25**) using the same protocol as for the preparation of DEX analogue **7** (Scheme 5). In the synthesis of 4,4′-(2-methylpropane-1,2-diyl)bis(piperazine-2,6-dione) (**10**), the corresponding tetraacetic acid **32** was prepared from 2-methyl-1,2-diaminopropane (**30**). Due to the sterically hindered amine in position 2, Strecker synthesis was used to prepare tetranitrile **31**, which was hydrolyzed to acid **32** as described previously.[44] Final cyclization in formamide gave only a low yield of product and several products of elimination were detected. Elimination proceeded, especially at the quaternary carbon in the linker. In the synthesis of *meso*-4,4′-(butane-2,3-diyl)bis(piperazine-2,6-dione) (**11**), known as ICRF-193, we started from the commercially available 2,3-butanediol **33**, while the ratio between meso form and

https://doi.org/10.1021/acs.jmedchem.0c02157
J. Med. Chem. 2021, 64, 3997−4019

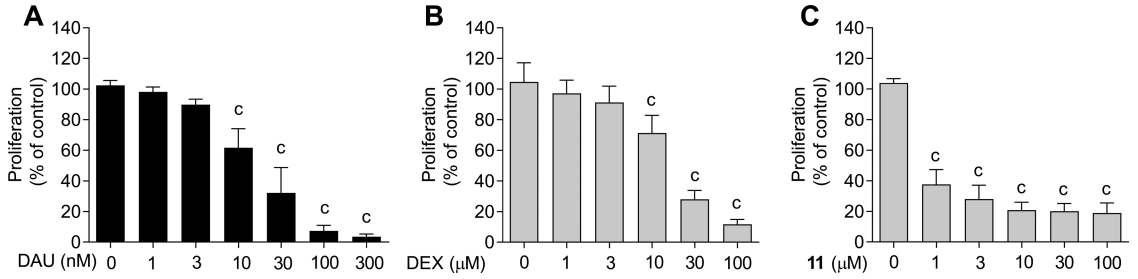

Figure 4. Antiproliferative activity of DAU, DEX, and compound **11** (ICRF-193). HL-60 cells were incubated for 72 h. The toxicity was assessed by the 2,3-bis-(2-methoxy-4-nitro-5-sulfophenyl)-2*H*-tetrazolium-5-carboxanilide (XTT) assay. Absorbances of the treatment wells were expressed as a percent of control wells. Data are presented as mean ± SD of four independent experiments. Statistical significance was determined in GraphPad Prism 8 using the one-way ANOVA with the Holm−Sidak *post hoc* test and was accepted at $P \leq 0.05$: c, significant to control.

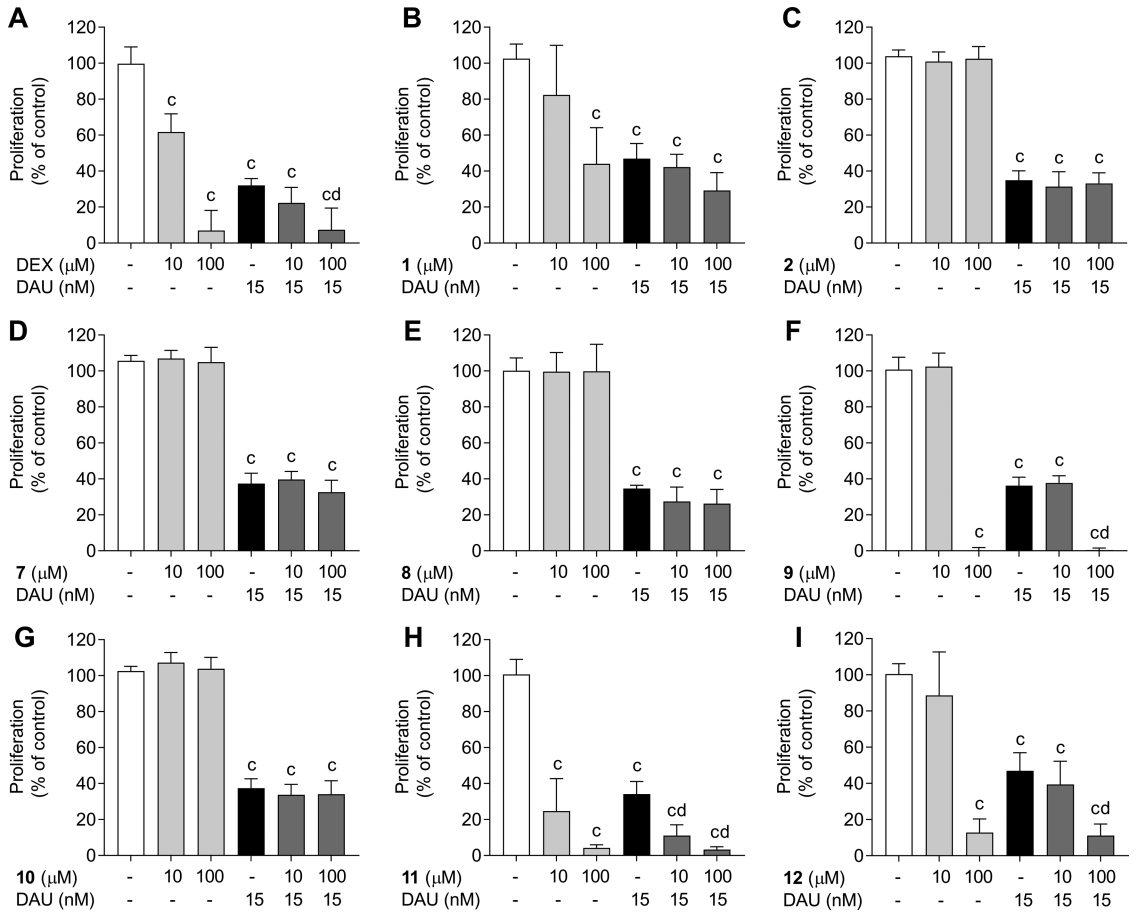

Figure 5. Antiproliferative activity of DEX and compounds **1**, **2**, and **7**−**12** and their influence on the antiproliferative effect of daunorubicin (DAU). HL-60 cells were incubated for 72 h with DEX and its analogues **1**, **2**, and **7**−**12** either alone (10 and 100 μM, light gray columns) or in combination with 15 nM DAU (dark gray columns for combinations, black columns for DAU alone). The toxicity was assessed by the XTT assay. Absorbances of the treatment wells were expressed as a percent of dimethyl sulfoxide (DMSO) control wells (white columns). Data are presented as mean ± SD of four independent experiments. Statistical significance was determined in GraphPad Prism 8 using the one-way ANOVA with the Holm−Sidak *post hoc* test and was accepted at $P \leq 0.05$: c, significant difference to untreated control and d, significant difference to DAU.

racemate in it was 2.5:1 according to NMR. Surprisingly, after the reduction of azide **35** to diamine and its conversion to dihydrochloride **36**, predominantly meso form crystallized from the reaction mixture and was isolated as 92% pure (8% was racemic form). Upon alkylation of diamine **36** with *tert*-butyl bromoacetate, both *meso*-tetraester **37a** and *rac*-tetraester **37b** were isolated using column chromatography. Then, in the cyclization step of tetraacetic acids **38a** and **38b**, a standard procedure in formamide under elevated temperatures was used. However, only *rac*-tetraacetic acid **38b** was successfully converted to *rac*-4,4′-(butane-2,3-diyl)bis(piperazine-2,6-dione) (**12**) using this method. For the cyclization of *meso*-tetraacetic acid **38a**, we used the cyclization procedure of its tetramethylester **39** in dioxane at room temperature as described previously.[29] Finally, *meso*-4,4′-(butane-2,3-diyl)bis-(piperazine-2,6-dione) (**11**) was prepared using a seven-step procedure in 14% overall yield (Scheme 5). As the meso-derivative **11** was later found to be a very potent TOP2B inhibitor and protectant of cardiomyocytes against ANT-induced toxicity, its presence in racemate **12** as an impurity

https://doi.org/10.1021/acs.jmedchem.0c02157
J. Med. Chem. 2021, 64, 3997−4019

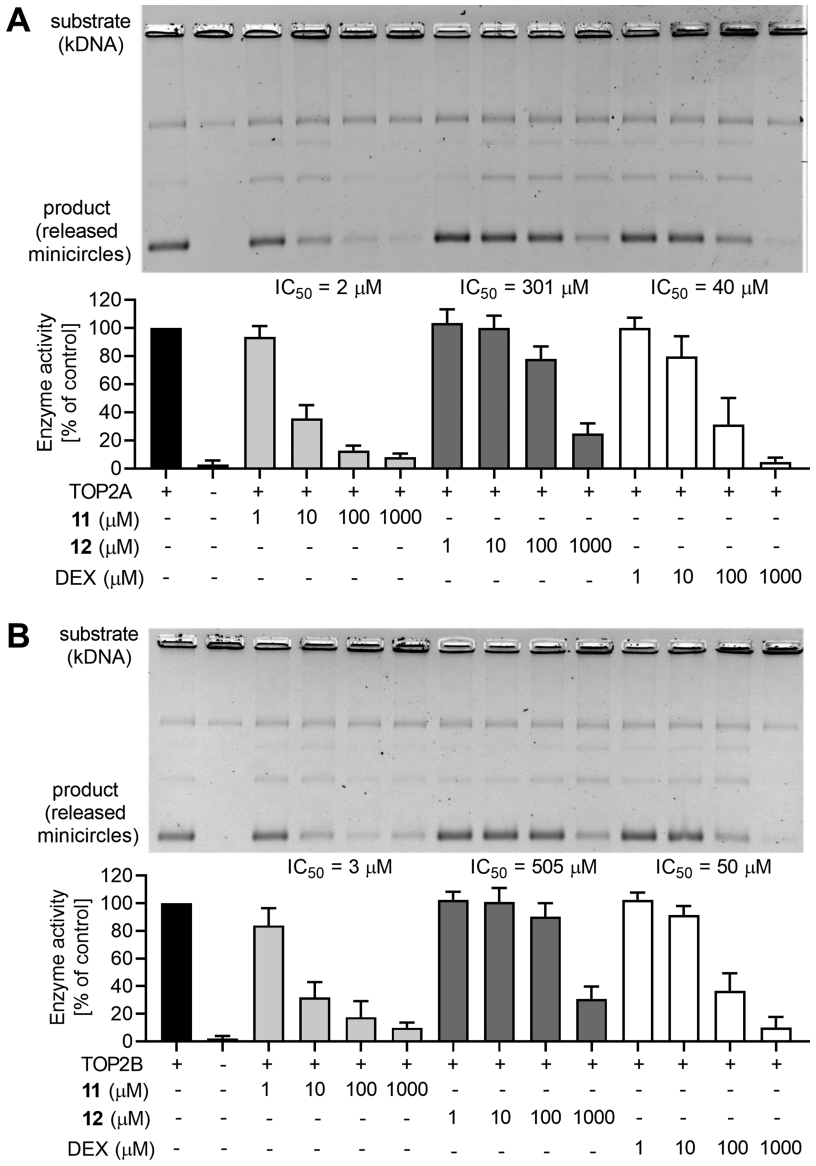

Figure 6. Concentration dependence of inhibition of recombinant human TOP2A (A) and TOP2B (B) by DEX and its analogues **11** and **12** (1−1000 μM). Isolated kDNA was incubated with either enzyme isoform in a reaction buffer and 1/10 volume of each compound diluted in 10% DMSO (final DMSO concentration 1%) for 30 min at 37 °C. In reactions performed in the presence of DEX, analogue **11** or **12** (1−1000 μM) are compared to the reaction with no TOP2 activity and with complete TOP2 activity. DMSO was added to the reactions where no other inhibitor was included in the same final concentration (1%). The signal of the treated samples was normalized to the respective control on the same gel (untreated sample, 100%), and the data are expressed as mean ± SD.

might have an impact on the results of the following *in vitro* studies. Therefore, we thoroughly analyzed the purity of racemate **12** using high-performance liquid chromatography-tandem mass spectrometry (HPLC-MS/MS) and found that it contained only a very low amount (0.035%) of its meso-form **11** (see Figure S6, Supporting Information).

***In Vitro* Assay of Cardioprotective Activity.** DEX and all its prepared analogues **1**−**12** were evaluated for their ability to protect primary cultures of rat neonatal ventricular cardiomyocytes (NVCMs) against daunorubicin (DAU)-induced toxicity. DAU (1.2 μM) treatment caused approximately 40−50% cytotoxicity (measured as the leakage of total intracellular lactate dehydrogenase (LDH) to the culture media; Figures 3 and S1, black columns). The protective activities of DEX and its analogues were assessed by the pretreatment of the culture for 3 h with subsequent cotreatment with DAU for 3 h (Figures 3 and S1, dark gray columns). This schedule was based on our previous findings and previously published literature.[30,45] The own toxicities of DEX and its analogues to NVCMs were also examined (Figures 3 and S1, light-gray columns).

All of the assessed agents were generally nontoxic on their own in the tested concentration range (10−100 μM). Apart from DEX, only four analogues displayed significant protective activity against DAU toxicity. Three of them, **8**, **9**, and **12**, were less effective than DEX. However, analogue **11** (ICRF-193) offered markedly better protection of NVCMs against DAU toxicity than DEX (significant protection was observed from 1 μM). Noteworthily, stereoisomers **11** and **12**, which differ just in the spatial orientation of methyl groups in the linker, showed significantly different potential to protect NVCMs, although stereoisomers DEX and LEV and their racemate were

https://doi.org/10.1021/acs.jmedchem.0c02157
J. Med. Chem. 2021, 64, 3997−4019

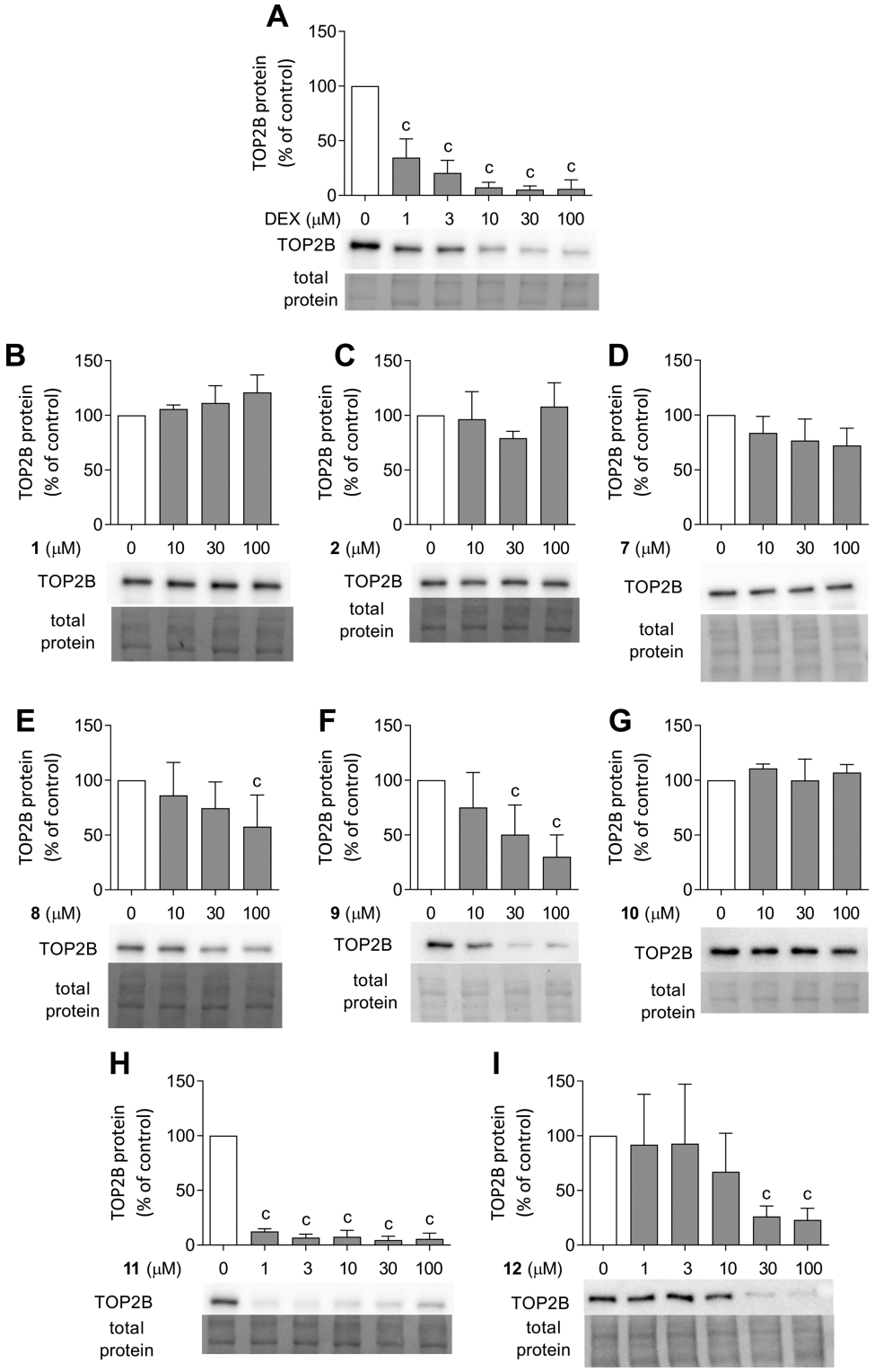

Figure 7. Depletion of TOP2B from neonatal rat ventricular cardiomyocytes. The cells were incubated with DEX or its analogues **1**, **2**, and **7**−**12** for 24 h, and TOP2B protein abundance was determined by immunoblotting with normalization to total protein using stain-free technology. The signal of the treated samples was normalized to the respective control on the same blot (untreated sample, 100%). The data of four independent experiments are expressed as mean ± SD. Statistical significance was determined using the one-way ANOVA with the Holm−Sidak *post hoc* test and was accepted at $P \leq 0.05$: c, significant difference to untreated control.

equally effective.[40] The EC_{50} value, *i.e.*, the concentration that reduced the toxicity of DAU toward cardiomyocytes to 50%, was 4 μM for meso-derivative **11**, while >100 μM for both DEX and rac-form **12**. Surprisingly, analogue **10** with high structural similarity to DEX and to both analogues **9** and **11** showed no significant protection or any nonsignificant trend toward this effect under the same conditions.

Inhibition of Proliferation of Leukemic Cells and the Effect on the Antiproliferative Activity of Daunorubicin. The antiproliferative effects of DEX and its analogues **1**−**12**

https://doi.org/10.1021/acs.jmedchem.0c02157
J. Med. Chem. 2021, 64, 3997−4019

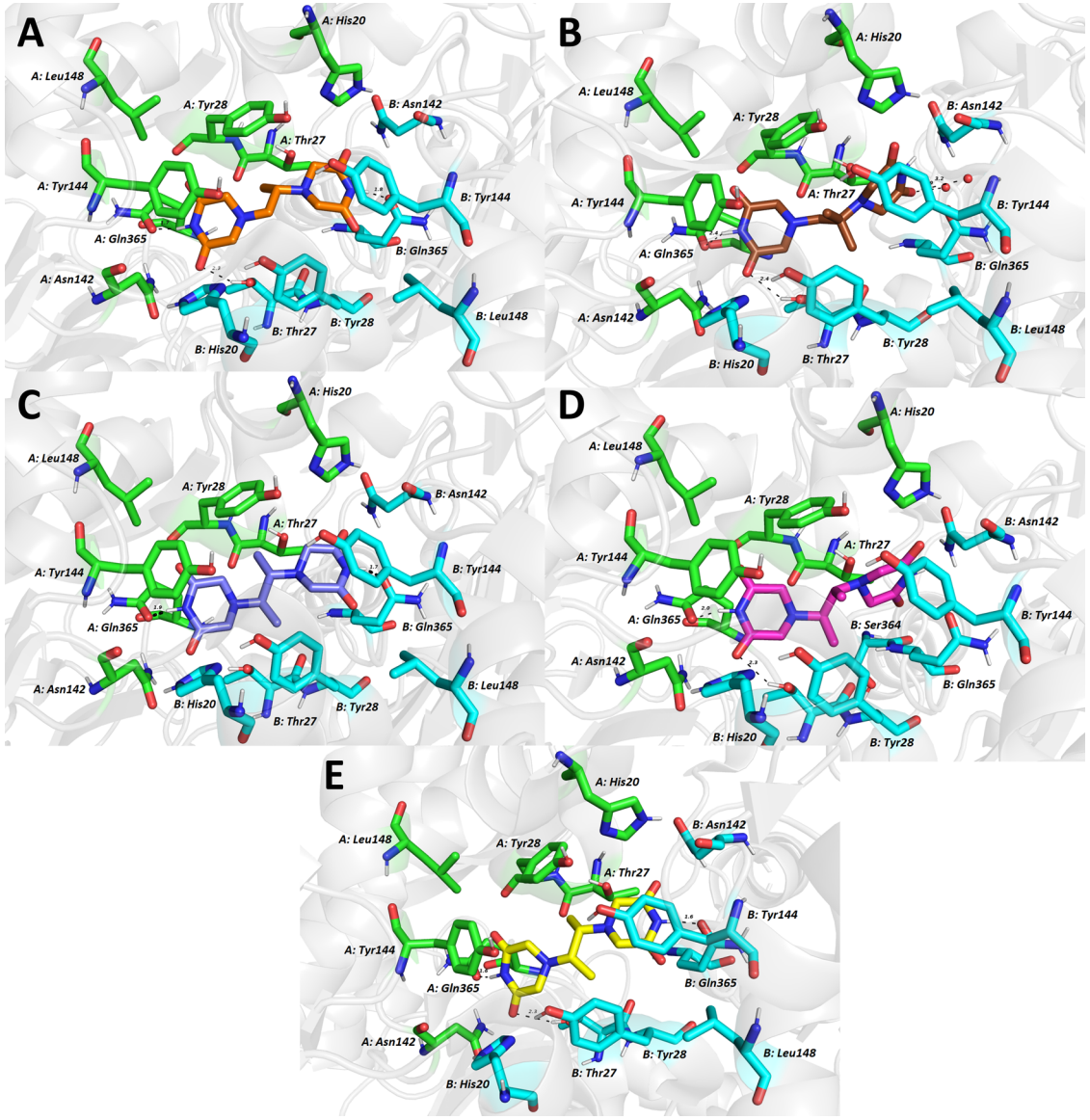

Figure 8. Crystal structure of DEX ((A) yeast, PDB ID: 1QZR)[14] and top-scored docking poses for **10** (B), *meso*-**11** (C), (*R*,*R*)-**12** (D), and (*S*,*S*)-**12** (E) in the DEX binding pocket of TOP2. The ligands are displayed in orange, brown, dark blue, purple, and yellow, respectively; important amino acid residues responsible for ligand anchoring are shown in green and light blue (the same color among residues determines a specific receptor protomer labeled either as "A" or "B"). Hydrogen bond contacts are rendered by black dashed lines; distances are measured in angstroms (Å). The rest of the receptor is displayed in the light-gray cartoon.

alone or in combination with DAU were studied in human leukemia HL-60 cell line. First, IC_{50} values of both DAU and DEX alone were assessed (15 nM and 18 μM, respectively; Figure 4). Then, the antiproliferative activity of DEX analogues was assessed in the same concentration ranges as in DEX (Figures 5 and S2; light gray columns) as limited solubility did not allow testing of higher concentrations in many analogues. The greatest inhibition of proliferation was seen in analogue **11** (IC_{50} = 0.037 μM, Figures 4C and 5H), and a significant effect was also noted in analogues **9** and **12**, although only in the highest concentration tested (100 μM, Figure 5F,I, respectively). However, it should be noted that the effects observed in the latter compound (**12**) could be partially attributed to the presence of a very low amount (0.035%) of highly potent meso-form **11** as an impurity (Figure S6). Analogue **8** was without any effect even in the highest concentration. Interestingly, analogues **1** and **6**, which had no activity in the cardioprotective assay (Figures 3B and S1D, respectively), also significantly inhibited proliferation of cancer cells at the highest assayed concentration (Figures 5B and S2D, respectively).

Then, the effects of DEX and its analogues on the antiproliferative activity of DAU were assessed. Most of the analogues had insignificant or weak effects on the proliferation of HL-60 cells, and IC_{50} values were often not reached and the classical Chou−Talalay analysis[46] could not be performed. Hence, we used low and high concentrations (10 and 100 μM, respectively) of the DEX and its analogues in combination with DAU in the calculated IC_{50} value (15 nM). The most important finding is that none of the tested compounds had any negative effect on the antiproliferative effect of DAU under the tested conditions, which is a clear prerequisite for their potential use as cardioprotective agents in the clinics. In contrast, significant enhancement of the antiproliferative effect of DAU was noted in DEX and analogues **6**, **9**, and **12** at 100

https://doi.org/10.1021/acs.jmedchem.0c02157
J. Med. Chem. 2021, 64, 3997−4019

μM, while compound **11** showed the enhancement effect at both 10 and 100 μM. To understand the mechanistic details of this observation, there will be a need to investigate the contribution of G2/M checkpoints known to be activated by TOP2 catalytic inhibitors, including ICRF-193 (**11**), because many cancer cells lack these cell cycle responses.[47,48]

Interactions with Topoisomerase II Isoforms. First, the inhibitory effects of DEX and its analogues **1**−**11** on the relaxation of supercoiled DNA by purified human recombinant TOP2 isoforms were studied in 1 mM final concentration (Figure S3A (TOP2A),B (TOP2B)). The final concentration was limited by the solubility of the compounds and the maximal amount of DMSO tolerable in the assay. Besides DEX, only the analogues **9** and **11** inhibited the recombinant enzymes, with a greater effect noticeable with analogue **11**. Detailed analysis of TOP2 inhibition by the analogues **11** and **12** showed roughly 1 order of magnitude higher potency of meso-derivative **11** compared to DEX, while rac-form **12** was roughly 1 order of magnitude less effective than DEX (Figure S3C (TOP2A),D (TOP2B)). These results closely correlated with the results obtained in another assay, where the inhibitory effects of DEX and its analogues **11** and **12** on the decatenation of kDNA by purified human recombinant TOP2 isoforms were studied and the respective IC_{50} values were calculated (Figure 6A (TOP2A),B (TOP2B)). Meso-derivative **11** was again found to be the strongest inhibitor of both TOP2A and TOP2B among the studied compounds with IC_{50} values of 2 and 3 μM, respectively. DEX showed approximately 10-times and racemic derivative **12** approximately 100-times lower potency as compared to meso-derivative **11**. All of the observed effects of DEX and its analogues **11** and **12** were the same for both TOP2 isoforms in both assays.

Previously, DEX and ICRF-193 were documented to induce depletion of TOP2 in various models *in vitro* and also *in vivo*.[30,36,49−51] Based on these results, we assessed the depletion of TOP2 in NVCMs after 24 h of incubation (Figures 7 and S4). The results of this assay correlated well with the results of the cardioprotective assay (Figures 3 and S1) and with the exception of compound **8** also with inhibition of purified recombinant TOP2A and TOP2B isoforms (Figures 6 and S3). The latter discrepancy may be explained by only a small effect of analogue **8** on the cardioprotective assay (Figure 3E) and a much longer time allowed for the depletion as compared to the TOP2 inhibition assay. This suggests that the TOP2 depletion assay may be more sensitive and may better correlate with the cardioprotection.

In accordance with cardioprotection and TOP2 inhibition, analogue **11** showed the strongest depletion of TOP2B (strong effect already at 1 μM), while its rac-form **12** or analogue **9** were only effective at concentrations $\geq$30 μM.

Molecular Modeling and Dynamic Simulation Studies. To explain the marked differences between DEX and its close analogues **10**, *meso*-**11**, and *rac*-**12** ((*R*,*R*)-**12** and (*S*,*S*)-**12**) in their ability to inhibit and deplete TOP2B in NVCMs, we have applied molecular modeling (Figure 8). As a receptor structure, we used yeast TOP2 (PDB ID: 1QZR).[14] The rationale for the choice of the receptor was dictated by (i) high resolution (1.90 Å) and (ii) absolute similarity of the respective ATP-binding sites and related DEX binding site between human TOP2B and yeast TOP2. The latter accounts for all of the critical residues involved in the anchoring of DEX in the TOP2 binding site in yeast.[14,52] To validate our model, we redocked DEX into the TOP2 DEX binding site, which showed a high degree of homology with an excellent root-mean-square deviation (RMSD) value of 0.4 Å, indicating high validity of the applied docking protocol (RMSD calculated with LigRMSD 1.0[53]). The superimposed structure of DEX from the crystal structure and docked DEX revealed a very close arrangement within the TOP2 DEX binding site. The only small difference between the docked DEX and the "bat-wing" conformation of DEX seen in the original crystal structure[14,54] can be found in the flipped conformation of one of the dioxopiperazine rings (Figure S5).

Our docking studies revealed that DEX interacts with the primary dimer interface formed by 14 amino acid residues (Figure 8A). DEX exerts only two hydrogen bonds between terminal imide hydrogens and Gln365 residues at distances of 1.7 and 1.8 Å. We have also found one additional hydrogen bond between the carbonyl oxygen of DEX and the hydroxyl group from Thr27 (2.3 Å). From the crystallography analysis, it is also evident that the attached methyl group at the ethylene linker is somewhat disordered, which generated two possible conformations (for the sake of clarity, we displayed only one conformer).[14] The most active meso-derivative **11** (Figure 8C) demonstrated an almost identical arrangement to that of DEX in the TOP2 DEX binding site, conveying two essential hydrogen bonds between carbonyl oxygens of Gln365 residues and terminal imide hydrogens (with distances of 1.9 and 1.7 Å). Most importantly, both methyl groups at the linker can contact their neighboring Tyr28 residues from each protomer *via* methyl−π interactions. In the case of DEX binding, this type of interaction is represented for only one Tyr28 residue. Stronger interaction of *meso*-**11** than DEX could also be explained by higher flexibility and related "entropic penalty" of DEX compared to *meso*-**11** after accommodation into the DEX binding site of TOP2. The conformation of *meso*-**11** is more rigid, and its dioxopiperazine units are naturally fixed in very beneficial positions.

Two protruding geminal methyl groups of analogue **10** (Figure 8B) placed one hydroxyl group from dioxopiperazine unit comparable to DEX or *meso*-**11** within the TOP2 binding pocket; however, the second dioxopiperazine stands aside from the Gln365 residue of the second protomer, providing hydrogen bonds with two water molecules only. Thus, complex **10**-TOP2 can be regarded as the least suitable for contacting both protomers simultaneously. Although other two stereoisomers, namely, (*R*,*R*)-**12** (Figure 8D) and (*S*,*S*)-**12** (Figure 8E), have been previously reported to be equally potent TOP2 inhibitors,[44] the docking results showed that in contrast to stereoisomer (*R*,*R*)-**12**, stereoisomer (*S*,*S*)-**12** unexpectedly adopted beneficial conformation very similar to that of DEX. Specifically, (*S*,*S*)-**12** established contact with both Gln365 residues, while (*R*,*R*)-**12** is linked to a single Gln365 residue only, since its linker imposes the second dioxopiperazine moiety to a less energetically favorable position. To further verify the results of the docking experiments, especially the unexpectedly positive result of compound (*S*,*S*)-**12**, we extended our docking analysis by molecular dynamics (MD) simulations (Figure 9). Similar to the docking results, MD indicated that DEX and meso-derivative **11** adopted nearly the same spatial arrangement in the TOP2 DEX binding site with apparent hydrogen bonds formed between carbonyl oxygens of Gln365 residues and terminal imide hydrogens. In addition, higher TOP2B inhibition activity of *meso*-**11** can be attributed to hydrophobic interactions of the protruding methyl in the

https://doi.org/10.1021/acs.jmedchem.0c02157
J. Med. Chem. 2021, 64, 3997−4019

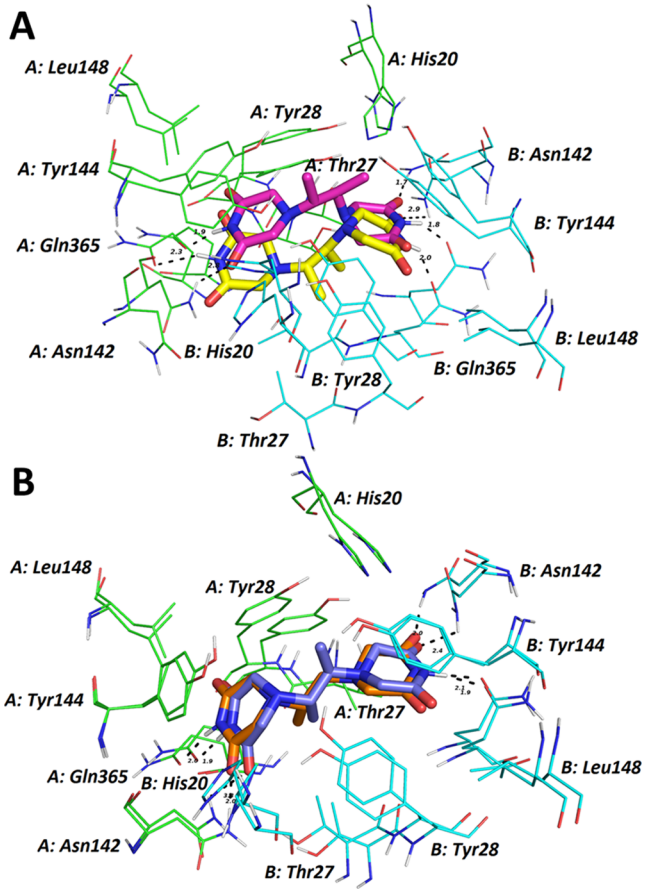

Figure 9. Molecular dynamic simulations of enantiomers (*R*,*R*)-**12** (panel (A); purple) and (*S*,*S*)-**12** (panel (A); yellow) and meso-derivative **11** (panel (B); blue) and DEX (panel (B); orange) in the DEX binding pocket of TOP2 (PDB ID: 1QZR).[14] Important amino acid residues responsible for ligand anchoring are shown in green and light blue lines (the same color among residues determines specific receptor protomer labeled either as "A" or "B"). Hydrogen bond contacts are rendered by black dashed lines; distances are measured in angstroms (Å).

linker (Figure 9B). In contrast to the docking results, the MD simulation revealed that both (*S*,*S*)-**12** and (*R*,*R*)-**12** enantiomers adopted significantly different and less beneficial arrangements compared to that of DEX or meso-derivative **11** (Figure 9A). Thus, the results of MD simulation of DEX, **11**, (*S*,*S*)-**12**, and (*R*,*R*)-**12** seem to correspond better with the experimental data than the results of docking analysis.

From the standpoint of *in silico* predictions, the activity of each ligand can be anticipated upon the linker stereochemistry along with the bulkiness of the attached moieties (methyl, ethyl, *etc.*). For all of the compounds selected for *in silico* studies (*i.e.*, DEX, **10**, *meso*-**11**, (*R*,*R*)-**12**, and (*S*,*S*)-**12**), their respective methyl groups at the ethylene linkers impact the conformation of the linker and the orientation of dioxopiperazine moieties mainly due to steric reasons, playing a critical role for the ligand binding to TOP2.

Displacement of Iron from the Complex with DAU. To assess whether the iron chelation activity of the tested compounds is linked to their pharmacological activity in cardiomyocytes and/or cancer cells, iron chelation was compared for DEX and analogues **1**, **2**, **11**, and **12** and their hydrolysis products ADR-925, **1-hp**, **2-hp**, **11-hp**, and **12-hp** (Figure 10C), respectively. The selection of these compounds was driven by their different pharmacological profiles in the above-mentioned bioassays—compound **1** showed slight antiproliferative effects (Figure 5B) and no cardioprotection (Figure 3B) and compound **2** showed no effect in either assay (Figures 3C and 5C). Compound **11** (ICRF-193) was more effective than DEX in both assays (Figures 3H and 5H), while its stereoisomeric form **12** was less effective than DEX in both assays (Figures 3I and 5I). The iron chelation activity of the parent compounds and their hydrolysis products was assessed by the displacement of the Fe^{3+} ions from the complex with DAU (Figure 10), which was used previously in similar studies.[55] As a positive control, a model experimental iron chelator salicylaldehyde isonicotinoyl hydrazone (SIH) was used, which displaced iron efficiently and almost completely.

As published before, the hydrolysis product of DEX, ADR-925, displaced Fe^{3+} ions from the complex with DAU effectively, contrary to DEX itself. The hydrolysis products of analogues **1** and **2**, primarily designed for this purpose, displaced Fe^{3+} even more efficiently than ADR-925. The analogue **2** displaced iron from the complex even after the addition of the parent compound (apparently due to its prompt hydrolysis). On the other hand, the hydrolysis product of analogue **11** was the least effective iron chelator despite being apparently the most effective in both cardioprotective and antiproliferative bioassays. The chelation efficiency of the hydrolysis product of its stereoisomeric counterpart—compound **12**—was comparable, although their cardioprotective efficiency was significantly different.

DISCUSSION

Initially, the iron chelation was the main hypothesis used to explain both antiproliferative and cardioprotective effects of bisdioxopiperazine agents. This was driven by the original design of (dex)razoxane as a cell-permeable prodrug of an EDTA-like chelator. In the case of cardioprotection, this notion was further strengthened by a coincidental description of iron-catalyzed prooxidative effects of ANTs in the heart.[55−58] Iron chelation was early questioned and finally disproved as the main mechanism of the antiproliferative effects of bisdioxopiperazines,[59] and the effects have been soon ascribed to the catalytic inhibition of TOP2.[6,7] ICRF-193 has been identified as the most potent TOP2 inhibitor and antiproliferative agents of this class.[17,18,60] However, the iron chelation remained an often cited theory of cardioprotective effects of DEX also used in documents issued by regulatory authorities.[28,61]

Analogue **1** (Figure 3), which differs from the previously described compound ICRF-161 just by the presence of the hydroxyl group in the aliphatic linker, completely lacked the activity in our cardioprotective bioassay. The hydrolysis product of **1** is a known commercial metal chelator; therefore, it was not a surprise that it effectively displaced Fe^{3+} ions from the complex with DAU in our present study. Analogue **1** is thus similar to ICRF-161 in the iron-chelating activity of its hydrolysis product and also in the lack of TOP2 inhibitory activity of the parent compound.[29] Noteworthily, both compound **1** studied herein and ICRF-161 tested previously show a complete lack of cardioprotective potential, which seems to be attributable to the impaired TOP2B interaction.[29] Hence, the prolongation of the linker is not a perspective modification of the DEX molecule regarding cardioprotective effects despite retained or even enhanced iron-chelating activity. The weak antiproliferative activity of bisdioxopiper-

https://doi.org/10.1021/acs.jmedchem.0c02157
J. Med. Chem. 2021, 64, 3997−4019

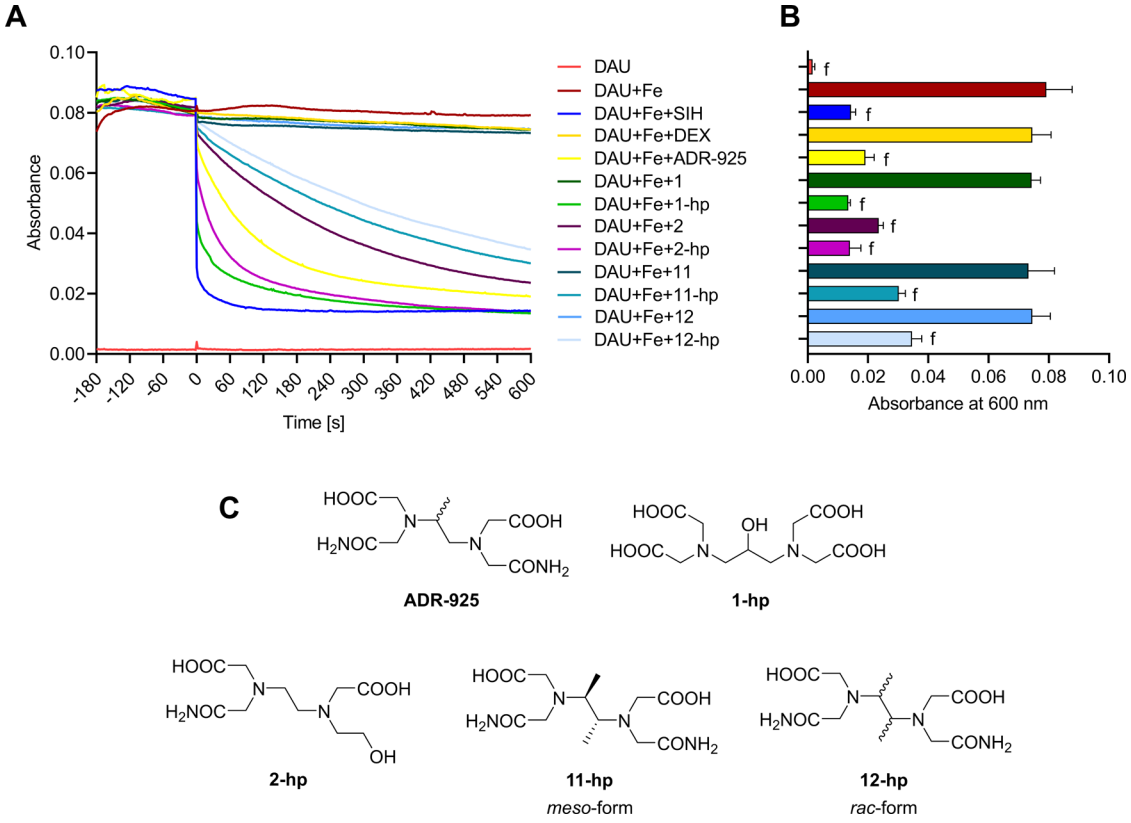

Figure 10. Displacement of Fe^{3+} from the DAU−Fe^{3+} complex measured as the absorbance change at λ = 600 nm. (A) Time profiles of the displacement—the data are presented as mean values, standard deviations were omitted for clarity. After 3 min of equilibration, the tested compounds (100 μM) or DMSO (solvent control) were added and the absorbance was monitored for 10 min. (B) The endpoint absorbances presented as means ± SD; statistical significance (one-way ANOVA, Holm−Sidak *post hoc* test $P \leq 0.05$; f, significantly different from DAU−Fe^{3+} complex). (C) Structure of the racemic form of ADR-925 and expected hydrolysis products **1-hp**, **2-hp**, **11-hp**, and **12-hp**.

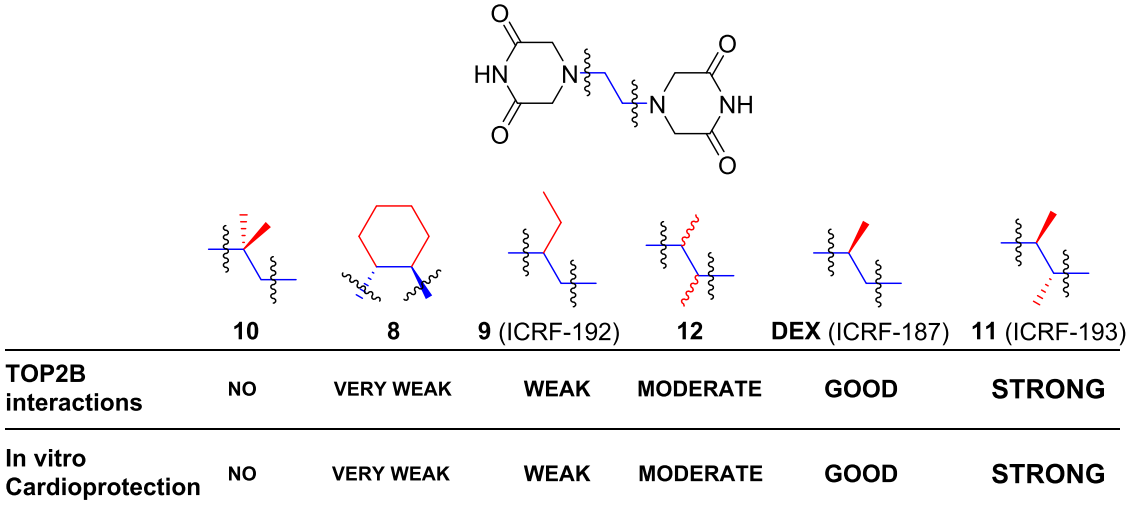

Figure 11. Structure−activity relationships of bisdioxopiperazines with respect to TOP2B inhibition/depletion and their cardioprotective activity.

azine **1** can be related to its iron chelation ability, as iron chelators are known for their antiproliferative effects.[62]

Compound **2** also produced a well-known metal-chelating metabolite, which displaced iron complexed with DAU even more effectively than ADR-925. Several other structurally related analogues evaluated in this study, *i.e.*, compounds **3** and **7**−**12**, are also very likely to be hydrolytically opened to EDTA-like iron-chelating metabolites. However, only compounds **8**, **9**, **11**, and **12** had the significant ability to protect NVCM cells against DAU toxicity. Importantly, the most potent cardioprotective agents in this study (**11**, ICRF-193) and its hydrolysis product **11-hp** were the least effective in the iron chelation assay, and their efficiency was roughly the same as those of their stereoisomeric counterparts **12** and **12-hp**, respectively. However, rac-form **12** showed markedly weaker cardioprotective activity than its meso-form **11**. All of the above-mentioned findings suggest that metal-chelating activities of bisdioxopiperazines and their metabolites do not

https://doi.org/10.1021/acs.jmedchem.0c02157
J. Med. Chem. 2021, 64, 3997−4019

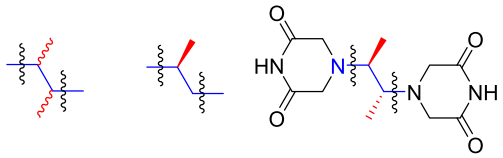

	12 racemate	DEX	11 (ICRF-193) meso-form
cardioprotection (EC_{50}, μM)	174	101	**4**
iron chelation (%)	57	77	63
TOP2B inhibition (IC_{50}, μM)	505	50	**3**

Figure 12. *In vitro* cardioprotective efficiency of DEX and stereoisomers **11** and **12** correlates with their inhibitory/depletory activity toward TOP2, not with their chelation potential.

correspond with cardioprotective effects observed in this and previous studies,[30,39,45] and thus metal chelation is unlikely to determine effective cardioprotection by bisdioxopiperazine derivatives.

Until the discovery of TOP2B, which is the predominant TOP2 isoform in cardiomyocytes,[34,35,63] TOP2 inhibition was not considered as a plausible mechanism for DEX cardioprotection. However, our present results obtained with DEX and its analogues **8**−**12** point to the key role of the inhibition/depletion of TOP2B in their cardioprotective activity. Cardioprotective potency observed in these experiments very closely mirrors their ability to inhibit and/or deplete TOP2, which is in accordance with the results of a recent study of Hasinoff.[52] From the SAR point of view, the substitution and configuration of the two-carbon linker between both dioxopiperazine rings were found to be the determining structural factors responsible for effective inhibition/depletion of TOP2B and related cardioprotective activity of DEX and its analogues **8**−**12** (Figure 11).

Achiral DEX analogue **10** with just one additional methyl on the original chiral carbon in the linker was unable to inhibit or deplete TOP2B, which was accompanied by the lack of the corresponding cardioprotective effects. Low cardioprotective potential of cyclohexyl analogue **8** and ethyl analogue **9** (ICRF-192), seen only at the highest tested concentration (Figure 3E,F, respectively), corresponded with the moderate depletion of TOP2B in cardiomyocytes (Figure 7) and in the case of slightly more potent analogue **9** also with the positive finding in the TOP2B inhibitory assay (Figure S3). Compound **11** (ICRF-193) has been found to be both the most potent TOP2 inhibitor and cardioprotectant against ANT toxicity, significantly surpassing clinically used DEX, as well as all previously tested bisdioxopiperazine derivatives. Markedly decreased ability of analogue **12**, *i.e.*, the stereoisomeric counterpart of the most active meso-derivative **11**, to inhibit TOP2B and to protect cardiomyocytes against ANT toxicity is among the strongest evidence that the cardioprotective efficiency of bisdioxopiperazines is TOP2B-dependent and not related to the chelation efficiency (Figure 12). Furthermore, the docking experiment provided a mechanistic explanation to this end. The substituents on the linker and their configuration were recognized to be essential for the effective interaction of bisdioxopiperazines with the DEX binding site of TOP2.

The remaining analogues **3**−**7**, which were inactive against TOP2B, as shown in Figures 7, S3, and S4, were also completely inactive as cardioprotectants. The example of analogue **7** confirms that the bulkier substitution on the two-carbon linker between both dioxopiperazine rings is detrimental for TOP2B activity and corresponding pharmacological effects. Regarding other modifications of the DEX molecule, it is apparent that the removal of just one oxo group from ICRF-154 in analogue **3**, *i.e.*, replacement of one imide by amide, completely deteriorates both the TOP2 interaction and correspondingly also the cardioprotective activity. This finding further supported our previous results that both imide groups were necessary for effective protection.[30] The replacement of dioxopiperazine cycles by a five-membered imidazolidine-2,4-dione or a succinimide ring in analogues **4**−**6** resulted in complete loss of activity in all assays employed in this study, although the distance of both imides in the analogue **6** is similar to DEX. Unfortunately, due to the chemical instability of succinimide-type analogues, we were not able to examine analogues with 1,2-diaminopropane or ethylenediamine linker, *i.e.*, the structures closer to parent DEX. Taken all together, the present data strongly indicate very narrow structure−activity relationships of bisdioxopiperazines with respect to both TOP2B inhibition and cardioprotection. The same is true for their TOP2A inhibition, which is in line with the well-documented mechanisms of antiproliferative effects. We have confirmed previously that TOP2A is not expressed in significant amounts in NVCMs used in this study;[63] therefore, its role in cardioprotective effects observed in the present study is highly unlikely.

The present study shows that ICRF-193 (*i.e.*, derivative in the meso-configuration) shows the highest cardioprotective potential. Previously, ICRF-193 (**11**) was not considered for further cardioprotective studies because it had been reported to be too toxic[1] and in an initial single-dose model the authors had reported no cardioprotection.[64] Hence, with respect to the former findings, a thorough analysis of cardioprotective effects and systemic toxicity in the *in vivo* model of chronic ANT toxicity is warranted. Given the increased potency of analogue **11** over DEX in our *in vitro* assays, optimal *in vivo* dose will have to be determined. However, the structural symmetry of the analogue **11** led to a sharp decrease of its solubility, which is the issue that must be resolved prior to future *in vivo* pharmacological evaluation as a potential cardioprotective drug candidate.

Considering that both ANTs and bisdioxopiperazines are TOP2 targeting compounds, there could be possible concerns about unwanted "prevention" of ANT toxicity also toward the cancer cells. This question becomes even more relevant given the indiscriminate inhibitory activity of DEX as well as other bisdioxopiperazines on both TOP2 isoforms seen in this study. Most importantly, in clinical settings, no reduction of ANT

https://doi.org/10.1021/acs.jmedchem.0c02157
J. Med. Chem. 2021, 64, 3997−4019

antineoplastic activity by DEX was found in multiple randomized clinical trials and their meta-analyses. Also, in our study, neither DEX, nor any of the analogues, including the most potent TOP2 inhibitor ICRF-193 (**11**), diminished the antiproliferative activity of DAU on leukemic cells.

CONCLUSIONS

In vitro evaluation of a series of DEX analogues showed that their cardioprotective activity tightly correlated with their ability to inhibit and deplete TOP2B in the NVCM cells. Furthermore, it revealed very narrow SAR between DEX and its cardioprotective activity, where the addition of even one methyl group substantially decreased or completely deteriorated the TOP2B inhibition and cardioprotective activity, as documented by the analogues **9** and **10**, respectively. The most efficient TOP2B inhibitor **11** (ICRF-193) also displayed the strongest depletory activity toward TOP2B and showed the most efficient protection of cardiomyocytes against ANT-induced toxicity. In contrast, its racemic stereoisomer **12** showed markedly decreased ability to inhibit TOP2B, which was accompanied by the decreased cardioprotective efficiency. Such tight SAR was further confirmed by docking analysis that showed the important role of the substituents on the linker and its configuration in the interaction with the DEX binding site of TOP2. However, the very low solubility of analogue **11** precludes rational *in vivo* evaluation; thus, a suitable formulation or a prodrug must be developed prior to the advanced *in vivo* studies. Our study also supported the recent findings that the iron-chelating efficiency of the studied compounds or their metabolites/hydrolysis products is not essential for their cardioprotective action and further highlighted the role of TOP2B in the pathogenesis of ANT cardiotoxicity.

EXPERIMENTAL SECTION

General. The structural identities of the prepared compounds were confirmed by ^{1}H NMR and ^{13}C NMR spectroscopy and by high-resolution mass spectrometry (HRMS). Each of the tested compounds had ≥95% purity, as determined using elemental analysis. All chemicals used for synthesis were obtained from Sigma-Aldrich (Schnelldorf, Germany) and were used as received. Thin-layer chromatography (TLC) was performed on Merck aluminum plates with silica gel 60 F_{254}. Merck Kieselgel 60 (0.040−0.063 mm) was used for column chromatography. Melting points were recorded with a Büchi B-545 apparatus (BUCHI Labortechnik AG, Flawil, Switzerland) and are uncorrected. ^{1}H and ^{13}C NMR spectra were recorded using a Varian Mercury VNMR S500 NMR spectrometer (Varian, Palo Alto, CA). Chemical shifts were reported as δ values in parts per million (ppm) and were indirectly referenced to tetramethylsilane (TMS) *via* the solvent signal. The elemental analysis was carried out on an Automatic Microanalyser EA1110CE (Fisons Instruments S.p.A., Milano, Italy). UHPLC system Acquity UPLC I-class (Waters, Milford) coupled to a high-resolution mass spectrometer (HRMS) Synapt G2Si (Waters, Manchester, U.K.) based on Q-TOF was used for the HRMS spectra measurement. Chromatography was performed using an Acquity BEH Shield RP18 (2.1 × 100 mm^2, 1.7 μm) column using gradient elution with 0.1% formic acid in water (A) and acetonitrile (B) at a flow-rate of 0.3 mL/min. Electrospray ionization (ESI) was operated in the positive mode. The ESI spectra were acquired in the range 50−1200 m/z using leucine−enkephalin as a lock mass reference and sodium formate for calibration. Tri(*tert*-butyl) 1,2-diaminoethane-*N*,*N*′,*N*′-triacetate (**15**) was prepared as described previously.[39] ADR-925 was prepared as described previously.[33]

Synthesis of 4,4′-(2-Hydroxypropane-1,3-diyl)bis(piperazine-2,6-dione) (1). 1,3-Diamino-2-hydroxypropane-*N*,*N*,*N*′,*N*′-tetraacetic acid (**13a**) (5 g, 15.5 mmol) was mixed with formamide (32 mL), and the reaction mixture was heated under reduced pressure (30 mbar) at 110 °C for 1.5 h. Then, the reaction flask was filled with argon and the reaction mixture was heated to 150−160 °C for 5 h. Upon completion, formamide was distilled off under reduced pressure (30 mbar). The residue was separated using column chromatography (mobile phase: EtOAc/acetone, gradient 25−100% acetone) and two crystalline products, 4,4′-(2-hydroxypropane-1,3-diyl)bis(piperazine-2,6-dione) (**1**) and 2-(2-((3,5-dioxopiperazin-1-yl)methyl)-6-oxomorpholino)acetamide (**1b**), were obtained. Both products were washed with methanol and dried.

*4,4′-(2-Hydroxypropane-1,3-diyl)bis(piperazine-2,6-dione) (**1**).* Yield: 14% as a white solid (R_f = 0.75, mobile phase: acetone); mp 173−175 °C; ^{1}H NMR (500 MHz, DMSO-d_6) δ 11.05 (s, 2H), 4.74 (d, J = 4.6 Hz, 1H), 3.82−3.75 (m, 1H), 3.36 (s, 8H), 2.45 (dd, J = 12.9, 4.3 Hz, 2H), 2.36 (dd, J = 12.9, 7.0 Hz, 2H). ^{13}C NMR (126 MHz, DMSO-d_6) δ 171.71, 66.35, 59.74, 56.01. Anal. calcd for $C_{11}H_{16}N_4O_5$: C, 46.48; H, 5.67; N, 19.71. Found: C, 46.69; H, 5.35; N, 19.62. HRMS (ESI$^+$) calcd for $(C_{11}H_{16}N_4O_5 + H)^+$ m/z: 285.11935; found: 285.1201.

*2-(2-((3,5-Dioxopiperazin-1-yl)methyl)-6-oxomorpholino)-acetamide (**1b**).* Yield: 34% as a white solid; (R_f = 0.3, mobile phase: acetone); mp 187−189 °C; ^{1}H NMR (500 MHz, DMSO-d_6) δ 11.14 (s, 1H), 7.42−7.28 (m, 1H), 7.25−7.06 (m, 1H), 4.80−4.60 (m, 1H), 3.48−3.36 (m, 5H), 3.25 (d, J = 17.3 Hz, 1H), 3.05−2.94 (m, 2H), 2.87 (dd, J = 12.3, 3.6 Hz, 1H), 2.79−2.69 (m, 2H), 2.55 (dd, J = 12.4, 7.9 Hz, 1H). ^{13}C NMR (126 MHz, DMSO-d_6) δ 171.44, 171.07, 167.27, 76.58, 58.94, 57.12, 55.68, 54.60, 51.23.

*4-(2-(2-Oxomorpholin-4-yl)ethyl)piperazine-2,6-dione (**2**).* *N*-(2-Hydroxyethyl)ethylenediamine-*N*,*N*′,*N*′-triacetic acid (**13b**) (16.5 g, 0.06 mol) was mixed with formamide (66 mL), and the reaction mixture was heated under reduced pressure (30 mbar) at 110 °C for 1.5 h. Then, the reaction flask was filled with argon and the reaction mixture was heated to 150−160 °C for 5 h. Upon completion, formamide was distilled off under reduced pressure (30 mbar), the residue was cooled to rt, and MeOH (30 mL) was added. The resulting suspension was stirred at rt overnight. The crystalline product was filtered, washed with another MeOH (50 mL), and dried in air. Yield: 39% (5.52 g) as a yellowish solid; mp 151−153 °C. ^{1}H NMR (500 MHz, DMSO-d_6) δ 11.05 (s, 1H), 4.29 (t, J = 5.1 Hz, 2H), 3.36 (s, 4H), 3.29 (s, 2H, overlapped with water), 2.69 (t, J = 5.1 Hz, 2H), 2.61 (t, J = 6.3 Hz, 2H), 2.52 (m, J = 6.2 Hz, 2H, overlapped with DMSO). ^{13}C NMR (126 MHz, DMSO-d_6) δ 171.62, 167.45, 68.59, 55.30, 55.24, 53.52, 51.90, 48.45. Anal. calcd for $C_{10}H_{15}N_3O_4$: C, 49.79; H, 6.27; N, 17.42. Found: C, 49.91; H, 6.48; N, 17.62. HRMS (ESI$^+$) calcd for $(C_{10}H_{15}N_3O_4 + H_2O + H)^+$ m/z: 260.12410; found: 260.1250.

Synthesis of 4-(2-(3-Oxopiperazin-1-yl)ethyl)piperazine-2,6-dione (3). *Tri(tert-butyl) N-(2-(tert-Butoxycarbonylamino)-ethyl)-1,2-diaminoethane-N,N′,N′-triacetate (**16**).* The mixture of tri(*tert*-butyl) 1,2-diaminoethane-*N*,*N*′,*N*′-triacetate (**15**) (2 g, 5 mmol), *tert*-butyl (2-bromoethyl)carbamate (1.34 g, 6 mmol), and potassium carbonate (0.89 g, 6.45 mmol) in CH_3CN (35 mL) was refluxed for 48 h. The reaction mixture was cooled down to rt and filtered. The filtrate was evaporated under reduced pressure, and the product **16** was isolated using column chromatography (mobile phase: hexane/EtOAc, 4:1). Yield: 1.5 g (55%) as a yellowish oil. ^{1}H NMR (500 MHz, $CDCl_3$) δ 5.69 (s, 1H), 3.44 (s, 4H), 3.30 (s, 2H), 3.15 (s, 2H), 2.86−2.60 (m, 6H), 1.45 (s, 27H), 1.43 (s, 9H). ^{13}C NMR (126 MHz, $CDCl_3$) δ 170.57, 156.21, 80.96, 78.64, 56.10, 55.87, 53.18, 52.32, 51.90, 38.50, 28.44, 28.12.

*4-(2-(3-Oxopiperazin-1-yl)ethyl)piperazine-2,6-dione (**3**).* Tri(*tert*-butyl) *N*-(2-(*tert*-butoxycarbonylamino)ethyl)-1,2-diaminoethane-*N*,*N*′,*N*′-triacetate **16** (1.5 g, 2.75 mmol) and hydrochloric acid (36%, 4.86 mL, 55 mmol) in H_2O (20 mL) was heated to 90 °C for 2 h. Then, the volatiles were evaporated under reduced pressure. The residue was mixed with formamide (5 mL) and heated under reduced pressure (30 mbar) at 110 °C for 1 h. Then, the reaction vessel was filled with argon and the reaction mixture was heated to 150−160 °C for 5 h. Formamide was distilled off under reduced

https://doi.org/10.1021/acs.jmedchem.0c02157
J. Med. Chem. 2021, 64, 3997−4019

pressure (30 mbar), and the product **3** was purified using column chromatography (mobile phase: $CHCl_3$/MeOH, 20:1). Yield: 0.15 g (24%) as a yellowish solid; mp 175−177 °C. ^{1}H NMR (500 MHz, DMSO-d_6) δ 11.07 (s, 1H), 7.70 (s, 1H), 3.36 (s, 4H, overlapped with water), 3.13−3.10 (m, 2H), 2.93 (s, 2H), 2.59 (t, J = 6.4 Hz, 2H), 2.57−2.52 (m, 2H), 2.51−2.45 (m, 2H). ^{13}C NMR (126 MHz, DMSO-d_6) δ 171.70, 167.89, 57.02, 55.40, 54.12, 52.13, 49.04, 40.49. Anal. calcd for $C_{10}H_{16}N_4O_3$: C, 49.99; H, 6.71; N, 23.32. Found: C, 50.24; H, 6.95; N, 23.11. HRMS (ESI$^+$) calcd for $(C_{10}H_{16}N_4O_3 + H)^+$ m/z: 241.12952; found: 241.1304.

Synthesis of 1,1′-(Propane-1,2-diyl)bis(imidazolidine-2,4-dione) (4). *(Propane-1,2-diyldiimino)diacetonitrile (18).* 1,2-Diaminopropane **17** (5 g, 0.067 mol) was cooled to 0 °C and glycolonitrile (55% in H_2O, 12 mL, 0.12 mol) was added dropwise. The reaction mixture was stirred at rt overnight. The resulting mixture was extracted with EtOAc (3 × 30 mL). The combined organic extracts were dried over anhydrous Na_2SO_4 and evaporated. The product **18** was purified using column chromatography (mobile phase: $CHCl_3$/MeOH, 25:1). Yield: 77% as a yellowish oil. ^{1}H NMR (500 MHz, $CDCl_3$) δ 3.71−3.52 (m, 4H), 2.99−2.92 (m, 1H), 2.89 (dd, J = 11.9, 3.5 Hz, 1H), 2.50 (dd, J = 11.9, 8.5 Hz, 1H), 1.09 (d, J = 6.5 Hz, 3H). ^{13}C NMR (126 MHz, $CDCl_3$) δ 117.93, 117.56, 53.61, 50.77, 37.08, 34.85, 17.61.

1,1′-(Propane-1,2-diyl)bis(imidazolidine-2,4-dione) (4). (Propane-1,2-diyldiimino)diacetonitrile (**18**) (7 g, 0.046 mol) was added to the solution of NaOH (5.5 g, 0.138 mol) in H_2O (20 mL) and the resulting mixture was heated to 80 °C for 3 h. Upon cooling, the reaction mixture was neutralized to pH = 7 using Amberlyst 15, filtered, and evaporated to dryness under reduced pressure to give 6 g of the crude 1,2-diaminopropane-*N*,*N*′-diacetic acid. The crude 1,2-diaminopropane-*N*,*N*′-diacetic acid (1 g) and KOCN (1.28 g, 15.8 mol) were heated in H_2O (7 mL) to reflux for 30 min. The reaction mixture was acidified to pH = 3 using aqueous HCl and heated to reflux for another 30 min. Then, the reaction mixture was cooled down and kept in the refrigerator at 4 °C for 1 week. The resulting crystalline product was filtered and recrystallized from water. Yield: 5% as a white solid; mp 265−267 °C. ^{1}H NMR (500 MHz, D_2O) δ 4.40−4.33 (m, 1H), 4.28−4.02 (m, 4H), 3.71 (dd, J = 14.9, 10.8 Hz, 1H), 3.17 (dd, J = 14.9, 3.7 Hz, 1H), 1.23 (d, J = 7.0 Hz, 3H). ^{1}H NMR (500 MHz, DMSO-d_6) δ 10.74 (s, 1H), 10.72 (s, 1H), 4.25−4.16 (m, 1H), 4.01−3.78 (m, 4H), 3.57 (dd, J = 14.5, 10.8 Hz, 1H), 2.95 (dd, J = 14.5, 3.8 Hz, 1H), 1.10 (d, J = 6.9 Hz, 3H). ^{13}C NMR (126 MHz, D_2O) δ 175.42, 175.16, 159.06, 158.86, 51.97, 47.50, 46.15, 45.26, 14.94. ^{13}C NMR (126 MHz, DMSO-d_6) δ 172.09, 171.90, 157.29, 157.13, 50.82, 46.42, 44.27, 44.01, 15.24. Anal. calcd for $C_9H_{12}N_4O_4$: C, 45.00; H, 5.04; N, 23.32. Found: C, 44.83; H, 5.18; N, 23.36. HRMS (ESI$^+$) calcd for $(C_9H_{12}N_4O_4 + H)^+$ m/z: 241.09313; found: 241.0937.

3,3′-(Hydrazine-1,2-diyl)bis(pyrrolidine-2,5-dione) (5). The solution of maleimide (1 g, 10.3 mmol) and hydrazine hydrate (0.257 g, 5.13 mmol) in 96% EtOH (20 mL) was stirred at rt for 72 h. The precipitated product was filtered and dried over P_2O_5. Yield: 69% as a white solid; mp 93−95 °C; ^{1}H NMR (500 MHz, DMSO-d_6) δ 11.06 (s, 2H), 4.65 (s, 0.9H), 4.58 (s, 1.1H), 3.86−3.75 (m, 2H), 2.82−2.67 (m, 2H), 2.61−2.50 (m, 2H). ^{13}C NMR (126 MHz, DMSO-d_6) δ 179.91, 179.57, 177.82, 177.46, 59.18, 59.00, 34.67, 34.14. Anal. calcd for $C_8H_{10}N_4O_4$: C, 42.48; H, 4.46; N, 24.77. Found: C, 42.31; H, 4.29; N, 24.5. HRMS (ESI$^+$) calcd for $(C_8H_{10}N_4O_4 + H)^+$ m/z: 227.07748; found: 227.0783.

N,N′-Bis(2,5-dioxopyrrolidin-3-yl)-N,N′-dimethylethylenediamine (6). *N*,*N*′-Dimethylethylenediamine (0.79 g, 0.97 mL, 9 mmol) was added in 10 portions over a period of 10 h into the stirred solution of maleimide (2 g, 20 mmol) in THF (5 mL) at rt. The resulting solution was further stirred for 12 h. THF was evaporated under reduced pressure and the product was purified using column chromatography (mobile phase: acetone). Yield: 38% as a yellowish solid; mp 118−120 °C. ^{1}H NMR (500 MHz, DMSO-d_6) δ 11.14 (s, 2H), 3.96 (dd, J = 8.9, 5.3 Hz, 2H), 2.68 (dd, J = 18.1, 8.9 Hz, 2H), 2.61−2.51 (m, 6H), 2.20 (d, J = 3.6 Hz, 6H). ^{13}C NMR (126 MHz, DMSO-d_6) δ 178.74, 176.97, 63.22, 63.16, 52.45, 52.36, 37.62, 37.54, 32.11, 32.08. Anal. calcd for $C_{12}H_{18}N_4O_4$: C, 51.06; H, 6.43; N, 19.85. Found: C, 50.97; H, 6.2; N, 19.74. HRMS (ESI$^+$) calcd for $(C_{12}H_{18}N_4O_4 + H)^+$ m/z: 283.14008; found: 283.1414.

Synthesis of 4,4′,4′′-(Propane-1,2,3-triyl)tris(piperazine-2,6-dione) (7). *Propane-1,2,3-triyl Trimethanesulfonate (20).* Methanesulfonyl chloride (43.55 g, 29.5 mL, 0.38 mol) was added dropwise to a solution of glycerol **19** (10 g, 8 mL, 0.11 mol) and triethylamine (38.4 g, 52.9 mL, 0.38 mol) in CH_3CN (250 mL) at 3 °C under an argon atmosphere. The reaction mixture was stirred at rt for 48 h and then filtered. The precipitate on the filter was washed with EtOAc (150 mL) and the filtrate was evaporated under reduced pressure. The crude product was dissolved in EtOAc (200 mL) and washed with water (2 × 200 mL) and brine (1 × 100 mL). The organic layer was evaporated to give a crude product **20**. Yield: 99% as a light brown oil. ^{1}H NMR (500 MHz, DMSO-d_6) δ 5.16 (tt, J = 5.9, 3.4 Hz, 1H), 4.50 (dd, J = 11.6, 3.4 Hz, 2H), 4.43 (dd, J = 11.6, 5.9 Hz, 2H), 3.29 (s, 3H), 3.27 (s, 6H). ^{13}C NMR (126 MHz, DMSO-d_6) δ 76.13, 67.63, 38.27, 37.05.

1,2,3-Triazidopropane (21). The mixture of propane-1,2,3-triyl trimethanesulfonate (**20**) (35 g, 0.107 mol) and sodium azide (20.87 g, 0.321 mol) in DMSO (200 mL) was stirred at 85 °C for 5 h under an argon atmosphere. Upon completion, water (600 mL) was added and the resulting solution was extracted with CH_2Cl_2 (4 × 100 mL). The combined organic extracts were washed with water (2 × 100 mL) and brine (1 × 100 mL), dried over anhydrous Na_2SO_4, and evaporated. The resulting 1,2,3-triazidopropane **21** was used in the next step without further purification. Yield: 91% as a yellow oil. ^{1}H NMR (500 MHz, $CDCl_3$) δ 3.70−3.64 (m, 1H), 3.53−3.41 (m, 4H). ^{13}C NMR (126 MHz, $CDCl_3$) δ 60.55, 51.94.

Propane-1,2,3-triamine Trihydrochloride (22). A solution of triazide **21** (16.3 g, 0.0975 mol) in EtOH (300 mL) under an argon atmosphere was refluxed and hydrazine hydrate (140 mL) and 5% Pd/C (1.5 g) were added in three portions over a period of 1.5 h at 0.5 h interval. The reaction mixture was heated to reflux for another 12 h, and then filtered through a pad of silica gel. The solvent was evaporated under reduced pressure to give the crude propane-1,2,3-triamine. The crude propane-1,2,3-triamine was dissolved in ethanol (150 mL) and 36% hydrochloric acid (20 mL) was added. This mixture was kept in a refrigerator at 4 °C for 48 h. The resulting suspension was filtered and propane-1,2,3-triamine trihydrochloride was dried over P_2O_5. Yield: 70% as a brown crystalline solid. ^{1}H NMR (500 MHz, D_2O) δ 3.96 (tt, J = 7.3, 5.2 Hz, 1H), 3.41 (dd, J = 14.4, 5.2 Hz, 2H), 3.35 (dd, J = 14.4, 7.3 Hz, 2H). ^{13}C NMR (126 MHz, D_2O) δ 46.86, 38.69.

Hexa(tert-butyl) 1,2,3-Triaminopropane-N,N,N′,N′,N′′,N′′-hexaacetate (23). The solution of propane-1,2,3-triamine trihydrochloride (1.5 g, 7.56 mmol), *tert*-butyl bromoacetate (9.58 g, 7.2 mL, 49.11 mmol), and K_2CO_3 (9.9 g, 71.63 mmol) in a mixture of THF (100 mL) and H_2O (20 mL) was refluxed for 25 h. The majority of THF was evaporated under reduced pressure and the residue was extracted with EtOAc (2 × 100 mL). The combined organic extracts were washed with water (2 × 200 mL), dried over anhydrous Na_2SO_4, and evaporated under reduced pressure. The product was purified using column chromatography (mobile phase: hexane/EtOAc, 15:1−3:1). Yield: 44% as a yellow oil. ^{1}H NMR (500 MHz, $CDCl_3$) δ 3.55−3.45 (m, 12H), 3.00−2.93 (m, 3H), 2.77−2.68 (m, 2H), 1.46 (s, 36H), 1.45 (s, 18H). ^{13}C NMR (126 MHz, $CDCl_3$) δ 171.39, 170.91, 80.57, 80.39, 60.37, 56.13, 54.77, 53.55, 28.18, 28.11.

4,4′,4′′-(Propane-1,2,3-triyl)tris(piperazine-2,6-dione) (7). Hexa(*tert*-butyl) 1,2,3-triaminopropane-*N*,*N*,*N*′,*N*′,*N*′′,*N*′′-hexaacetate **23** (6.3 g, 8.1 mmol) and 36% aq. HCl (50 mL) in H_2O (50 mL) was heated to 90 °C for 4.5 h. Then, all of the volatiles were evaporated under reduced pressure to give the crude 1,2,3-triaminopropane-*N*,*N*,*N*′,*N*′,*N*′′,*N*′′-hexaacetic acid trihydrochloride. The crude 1,2,3-triaminopropane-*N*,*N*,*N*′,*N*′,*N*′′,*N*′′-hexaacetic acid trihydrochloride was mixed with formamide (24 mL), and the reaction mixture was heated under reduced pressure (34 mbar) to 115 °C for 1.5 h. Then, the reaction vessel was filled with argon and the reaction mixture was heated for another 5 h at 150−160 °C under an argon atmosphere. Upon completion, formamide was distilled off under reduced pressure

https://doi.org/10.1021/acs.jmedchem.0c02157
J. Med. Chem. 2021, 64, 3997−4019

(34 mbar), the residue was cooled to rt and MeOH (20 mL) was added. The resulting beige precipitate was filtered, washed with cold methanol (20 mL), and dried in air. Yield: 40% as a brownish solid; mp 230−232 °C. ^{1}H NMR (500 MHz, DMSO-d_6) δ 11.08 (s, 2H), 10.95 (s, 1H), 3.50 (s, 4H), 3.42−3.25 (m, 8H, overlapped with water), 2.57−2.50 (m, 3H, overlapped with DMSO), 2.35 (dd, J = 13.2, 5.5 Hz, 2H). ^{13}C NMR (126 MHz, DMSO-d_6) δ 172.12, 171.59, 55.29, 55.00, 51.71. Anal. calcd for $C_{15}H_{20}N_6O_6$: C, 47.37; H, 5.30; N, 22.10. Found: C, 47.41; H, 5.39; N, 22.37. HRMS (ESI$^+$) calcd for $(C_{15}H_{20}N_6O_6 + H)^+$ m/z: 381.15171; found: 381.1521.

*trans-4,4′-(Cyclohexane-1,2-diyl)bis(piperazine-2,6-dione) (**8**).* *trans*-1,2-Cyclohexanediamine-*N,N,N′,N′*-tetraacetic acid monohydrate **24** (10 g, 3.13 mmol) was mixed with formamide (40 mL), and the reaction mixture was heated under reduced pressure (30 mbar) at 110 °C for 1.5 h. Then, the reaction vessel was filled with argon and the reaction mixture was heated for another 5 h at 150−160 °C under an argon atmosphere. Upon completion, formamide was distilled off under reduced pressure (30 mbar), the residue was cooled to rt and MeOH (20 mL) was added. The resulting suspension was stirred at rt overnight. The crystalline product was filtered, washed with another MeOH (25 mL), and dried. Yield: 57% as a white solid; mp 313−315 °C. ^{1}H NMR (500 MHz, DMSO-d_6) δ 10.93 (s, 2H), 3.50−3.34 (m, 8H), 2.75−2.65 (m, 2H), 1.74−1.57 (m, 4H), 1.22−1.04 (m, 4H). ^{13}C NMR (126 MHz, DMSO-d_6) δ 172.29, 60.99, 51.77, 26.52, 24.80. Anal. calcd for $C_{14}H_{20}N_4O_4$: C, 54.54; H, 6.54; N, 18.17. Found: C, 54.15; H, 6.28; N, 18.09. HRMS (ESI$^+$) calcd for $(C_{14}H_{20}N_4O_4 + H)^+$ m/z: 309.15573; found: 309.1568.

Synthesis of 4,4′-(Butane-1,2-diyl)bis(piperazine-2,6-dione) (9). *Butane-1,2-diyl Dimethanesulfonate (**26**).* Methanesulfonyl chloride (55.93 g, 38 mL, 0.488 mol) was added dropwise to a solution of 1,2-butanediol **25** (20 g, 13.91 mL, 0.222 mol) and triethylamine (49.3 g, 68 mL, 0.488 mol) in CH_2Cl_2 (250 mL) at 5 °C under an argon atmosphere. The reaction mixture was stirred at rt for 48 h. Upon completion, the reaction mixture was filtered and the solid on the filter was washed with another CH_2Cl_2 (100 mL). The organic filtrate was washed with saturated solution of $NaHCO_3$ (1 × 250 mL) and water (2 × 150 mL), dried over anhydrous Na_2SO_4, and evaporated under reduced pressure. Yield: 76%. ^{1}H NMR (500 MHz, $CDCl_3$) δ 4.86−4.79 (m, 1H), 4.40 (dd, J = 11.5, 3.0 Hz, 1H), 4.29 (dd, J = 11.5, 6.4 Hz, 1H), 3.09 (s, 3H), 3.08 (s, 3H) 1.84−1.76 (m, 2H), 1.05 (t, J = 7.5 Hz, 3H). ^{13}C NMR (126 MHz, $CDCl_3$) δ 80.30, 69.20, 38.68, 37.69, 24.37, 9.23.

*1,2-Diazidobutane (**27**).* Mixture of butane-1,2-diyl dimethanesulfonate **26** (39.4 g, 0.17 mol) and sodium azide (33 g, 0.51 mol) in DMSO (300 mL) was heated under an argon atmosphere at 85 °C for 5 h. Upon completion, water (600 mL) was added and the resulting solution was extracted with CH_2Cl_2 (4 × 100 mL). The combined organic extracts were washed with water (2 × 100 mL) and brine (1 × 300 mL), dried over anhydrous Na_2SO_4, and evaporated. The resulting 1,2-diazidobutane **27** was used in the next step without further purification. Yield: 60% as a yellowish oil. ^{1}H NMR (500 MHz, $CDCl_3$) δ 3.45−3.37 (m, 2H), 3.35−3.29 (m, 1H), 1.69−1.51 (m, 2H), 1.03 (t, J = 7.4 Hz, 3H). ^{13}C NMR (126 MHz, $CDCl_3$) δ 63.41, 54.42, 24.92, 10.27.

*Tetra(tert-butyl) 1,2-Diaminobutane-N,N,N′,N′-tetraacetate (**28**).* Ten percent of Pd on activated carbon (4.2 g, 3.9 mmol, 5 mol %) was added to the solution of 1,2-diazidobutane **27** (11 g, 0.0785 mol) in MeOH (250 mL) under an argon atmosphere. The reaction mixture was stirred in a hydrogen atmosphere (1 atm, balloon) for 14 days (hydrogen was replenished every second day). Upon completion, the reaction mixture was filtered and the solvent was evaporated under reduced pressure. The residue was dissolved in the mixture of THF and H_2O, 5:1 (300 mL) and *tert*-butyl bromoacetate (39.6 g, 29.7 mL, 0.203 mol) and potassium carbonate (29.6 g, 0.214 mol) were added. The reaction mixture was refluxed for 12 h. Upon completion, the reaction mixture was cooled down, the majority of THF was evaporated and the residue was extracted with EtOAc (2 × 100 mL). The combined organic extracts were washed with water (2 × 200 mL), dried over anhydrous Na_2SO_4, and evaporated under reduced pressure. The product **28** was purified using column chromatography (mobile phase: hexane/EtOAc, 20:1 → 5:1). Yield: 29%. ^{1}H NMR (500 MHz, $CDCl_3$) δ 3.50−3.38 (m, 8H), 2.89 (dd, J = 13.4, 6.0 Hz, 1H), 2.70 (p, J = 6.5 Hz, 1H), 2.54−2.44 (m, 1H), 1.53−1.37 (m, 38H), 0.95 (t, J = 7.4 Hz, 3H). ^{13}C NMR (126 MHz, $CDCl_3$) δ 171.60, 170.83, 80.71, 80.39, 62.49, 56.39, 56.00, 53.29, 28.14, 28.08, 23.65, 11.43.

*1,2-Diaminobutane-N,N,N′,N′-tetraacetic Acid Dihydrochloride (**29**).* Ester **28** (12.3 g, 0.0226 mol) and 36% aq. HCl (40 mL, 0.465 mmol) in H_2O (40 mL) was heated to 90 °C for 4 h. All of the volatiles were evaporated under reduced pressure. The product **29** was dried over P_2O_5. Yield: 97% as a white solid. ^{1}H NMR (500 MHz, DMSO-d_6) δ 3.93−3.77 (m, 8H), 3.42−3.32 (m, 1H), 3.24 (dd, J = 14.4, 3.5 Hz, 1H), 3.05 (dd, J = 14.3, 11.9 Hz, 1H), 1.79−1.68 (m, 1H), 1.40−1.25 (m, 1H), 0.87 (t, J = 7.4 Hz, 3H). ^{13}C NMR (126 MHz, DMSO-d_6) δ 170.76, 170.65, 62.64, 54.60, 53.54, 52.55, 19.61, 11.00.

*4,4′-(Butane-1,2-diyl)bis(piperazine-2,6-dione) (**9**).* Tetraacetic acid **29** (8.6 g, 0.022 mol) was mixed with formamide (35 mL), and the reaction mixture was heated under reduced pressure (30 mbar) at 110 °C for 1.5 h. Then, the reaction vessel was filled with argon and the reaction mixture was heated under an argon atmosphere to 150−160 °C for another 5 h. Upon completion, formamide was distilled off under reduced pressure (30 mbar), the residue was cooled to rt, and MeOH (20 mL) was added. The resulting suspension was stirred at rt overnight. The crystalline product was filtered, washed with another MeOH (25 mL), and dried over P_2O_5. Yield: 44% as a white solid; mp 213−215 °C. ^{1}H NMR (500 MHz, DMSO-d_6) δ 11.07 (s, 1H), 10.96 (s, 1H), 3.48−3.38 (m, 4H), 3.38−3.26 (m, 4H, overlapped with water), 2.84−2.74 (m, 1H), 2.62 (dd, J = 13.3, 8.5 Hz, 1H), 2.28 (dd, J = 13.3, 4.7 Hz, 1H), 1.36 (dt, J = 14.5, 7.3 Hz, 1H), 1.24 (dt, J = 14.0, 6.9 Hz, 1H), 0.83 (t, J = 7.4 Hz, 3H). ^{13}C NMR (126 MHz, DMSO-d_6) δ 172.22, 171.56, 59.34, 55.76, 55.34, 51.72, 21.90, 11.41. Anal. calcd for $C_{12}H_{18}N_4O_4$: C, 51.06; H, 6.43; N, 19.85. Found: C, 50.93; H, 6.25; N, 19.74. HRMS (ESI$^+$) calcd for $(C_{12}H_{18}N_4O_4 + H)^+$ m/z: 283.14008; found: 283.1411.

Synthesis of 4,4′-(2-Methylpropane-1,2-diyl)bis(piperazine-2,6-dione) (10). *2-Methyl-1,2-diaminopropane-N,N,N′,N′-tetraacetonitrile (**31**).*[44] 2-Methyl-1,2-diaminopropane **30** (4.4 g, 0.05 mol) was cooled in the ice bath and aqueous formaldehyde (37%, 20.3 g, 0.25 mol), 50% aqueous H_2SO_4 (35 g, 0.175 mol), and sodium cyanide (12.25 g, 0.25 mol) in H_2O (22 mL) were subsequently added dropwise under vigorous stirring. Then, the reaction mixture was stirred and heated to 35 °C for 40 h. Upon completion, the reaction mixture was cooled down and kept in the refrigerator overnight. The resulting crude product was filtered and recrystallized from water. Yield: 19%. ^{1}H NMR (500 MHz, DMSO-d_6) δ 3.92 (s, 4H), 3.86 (s, 4H), 2.59 (s, 2H), 1.16 (s, 6H). ^{13}C NMR (126 MHz, DMSO-d_6) δ 118.28, 116.48, 59.26, 59.11, 44.13, 37.33, 22.43.

*2-Methyl-1,2-diaminopropane-N,N,N′,N′-tetraacetic Acid (**32**).*[44] Compound **31** (2.33 g, 9.5 mmol) and $Ba(OH)_2{\cdot}8H_2O$ (7.5 g, 23.8 mmol) were heated in water (30 mL) to reflux for 24 h. The reaction mixture was cooled down, placed in the ice bath, and H_2SO_4 (96%, 2.42 g, 23.8 mmol) was added dropwise. A hot mixture with precipitated $BaSO_4$ was filtered and clear filtrate was evaporated under reduced pressure to obtain a yellow crystalline product. The final product **32** was recrystallized from water. Yield: 58% as a white solid. ^{1}H NMR (500 MHz, DMSO-d_6) δ 12.40 (br s, 1H), 3.56 (s, 4H), 3.45 (s, 4H), 2.65 (s, 2H), 0.98 (s, 6H). ^{13}C NMR (126 MHz, DMSO-d_6) δ 175.42, 173.00, 61.91, 58.94, 56.40, 53.16, 23.38.

*4,4′-(2-Methylpropane-1,2-diyl)bis(piperazine-2,6-dione) (**10**).* Compound **32** (1 g, 3.12 mmol) was mixed with formamide (4 mL), and the reaction mixture was heated under reduced pressure (30 mbar) at 110 °C for 1.5 h. Then, the reaction vessel was filled with argon and the reaction mixture was heated at 150−160 °C under an argon atmosphere for another 5 h. Upon completion, formamide was distilled off under reduced pressure (30 mbar), the residue was cooled to rt and MeOH (2 mL) was added. The solvent was evaporated, and the product **10** was purified using column chromatography ($CHCl_3$/

https://doi.org/10.1021/acs.jmedchem.0c02157
J. Med. Chem. 2021, 64, 3997−4019

MeOH, 20:1). The isolated product was washed with MeOH and dried. Yield: 18% as a white solid; mp 205−207 °C. ^{1}H NMR (500 MHz, DMSO-d_6) δ 11.09 (s, 1H), 11.08 (s, 1H), 3.41 (s, 4H), 3.34 (s, 4H), 2.44 (s, 2H), 0.99 (s, 6H). ^{13}C NMR (126 MHz, DMSO-d_6) δ 172.19, 171.88, 60.88, 57.35, 57.05, 50.02, 21.51. Anal. calcd for $C_{12}H_{18}N_4O_4$: C, 51.06; H, 6.43; N, 19.85. Found: C, 51.17; H, 6.37; N, 19.62. HRMS (ESI$^+$) calcd for $(C_{12}H_{18}N_4O_4 + H)^+$ m/z: 283.14008; found: 283.1407.

Synthesis of *meso*-4,4′-(Butane-2,3-diyl)bis(piperazine-2,6-dione) (11) and *rac*-4,4′-(Butane-2,3-diyl)bis(piperazine-2,6-dione) (12). *Butane-2,3-diyl Dimethanesulfonate (**34**).* To a solution of 2,3-butanediol **33** (mixture of isomers, 20 g, 0.22 mol) and triethylamine (56 g, 77 mL, 0.55 mol) in CH_2Cl_2 (600 mL), methanesulfonyl chloride (63.55 g, 43 mL, 0.55 mol) was added dropwise under an argon atmosphere. The reaction mixture was stirred for 2 h. The reaction mixture was washed with water (2 × 400 mL), saturated $NaHCO_3$ (1 × 400 mL), and again with water (1 × 400 mL). The organic layer was dried over anhydrous sodium sulfate and the solvent was evaporated under reduced pressure. Yield: 99% as a yellowish oil. The ratio of *meso*-butane-2,3-diyl dimethanesulfonate and *rac*-butane-2,3-diyl dimethanesulfonate was 2.5:1 according to ^{1}H NMR. Meso form; ^{1}H NMR (500 MHz, $CDCl_3$) δ 4.94−4.86 (m, 2H), 3.09 (s, 6H), 1.44 (d, J = 6.6 Hz, 6H). ^{13}C NMR (126 MHz, $CDCl_3$) δ 78.93, 38.61, 15.88. Rac form; ^{1}H NMR (500 MHz, $CDCl_3$) δ 4.81−4.74 (m, 0.78H), 3.08 (s, 2.32H), 1.47 (d, J = 6.2 Hz, 2.15H). ^{13}C NMR (126 MHz, $CDCl_3$) δ 78.66, 38.75, 17.19.

*2,3-Diazidobutane (**35**).* The mixture of butane-2,3-diyl dimethanesulfonate (mixture of isomers, 54 g, 0.22 mol) and sodium azide (61 g, 0.94 mol) in DMF (550 mL) was heated to 85 °C for 6 h. The reaction mixture was cooled down and diluted with water (1000 mL). The mixture was extracted with Et_2O (5 × 200 mL). The combined organic extracts were additionally washed with water (2 × 100 mL). Most of the solvent was evaporated on a rotary evaporator at 40 °C (water bath) and 300 mbar. As 2,3-diazidobutane **35** is volatile and potentially explosive, it was not completely dried from the rest of the solvents and was used without further purification in the next step. Yield: 32.7 g of a crude product as a yellowish oil. The ratio of *meso*-2,3-diazidobutane and *rac*-2,3-diazidobutane was 2.8:1 according to ^{1}H NMR. Meso form; ^{1}H NMR (500 MHz, $CDCl_3$) δ 3.52−3.46 (m, 2H), 1.29 (d, J = 6.5 Hz, 6H). ^{13}C NMR (126 MHz, $CDCl_3$) δ 60.91, 15.01. Rac form; ^{1}H NMR (500 MHz, $CDCl_3$) δ 3.45−3.40 (m, 0.7H), 1.31 (d, J = 6.5 Hz, 2.15H). ^{13}C NMR (126 MHz, $CDCl_3$) δ 61.07, 15.90.

*2,3-Butanediamine Dihydrochloride (**36**).* 10% Pd on activated carbon (11.7 g, 0.011 mmol, 5 mol %) was added to a 1000 mL flask and the flask was filled with Ar. Then, the solution of the crude 2,3-diazidobutane **35** (32.7 g) in MeOH (500 mL) was added. The reaction mixture was stirred in a hydrogen atmosphere (hydrogen was replenished once a week) for 1 month. The reaction was filtered and the filtrate was saturated with HCl (gas). The reaction mixture was kept in the refrigerator at 4 °C for 2 days. The resulting crystalline product was filtered and washed with Et_2O to obtain 13.25 g of *meso*-2,3-butanediamine dihydrochloride as a yellow solid. Yield: 38% over two steps from compound **34**. The ratio of *meso*-2,3-butanediamine and *rac*-2,3-butanediamine dihydrochlorides was 12:1 according to ^{1}H NMR. *Meso*-2,3-butanediamine dihydrochloride; ^{1}H NMR (500 MHz, D_2O) δ 3.62−3.55 (m, 2H), 1.35 (d, J = 6.8 Hz, 6H). ^{13}C NMR (126 MHz, D_2O) δ 49.62, 14.36. *rac*-2,3-Butanediamine dihydrochloride; ^{1}H NMR (500 MHz, D_2O) δ 3.72−3.65 (m, 0.18H), 1.30 (d, J = 6.7 Hz, 0.5H). ^{13}C NMR (126 MHz, D_2O) δ 48.50, 12.17.

*meso-Tetra(tert-butyl) 2,3-Diaminobutane-N,N,N′,N′-tetraacetate (**37a**) and rac-Tetra(tert-butyl) 2,3-Diaminobutane-N,N,N′,N′-tetraacetate (**37b**).* The solution of *meso*-2,3-butanediamine dihydrochloride **36** (8.2 g, 0.051 mol), *tert*-butyl bromoacetate (44.68 g, 33.6 mL, 0.23 mol) and K_2CO_3 (42 g, 0.3 mol) in the mixture of THF (250 mL) and H_2O (50 mL) was refluxed for 24 h. The majority of THF was evaporated under reduced pressure. The residue was extracted with EtOAc (3 × 100 mL). The combined organic extracts were additionally washed with water (2 × 100 mL). The organic layer was dried over anhydrous Na_2SO_4 and evaporated under reduced pressure.

The product **37a** was purified using column chromatography (mobile phase: hexane/EtOAc, 20:1 → 1:1). Yield: 76% (21.1 g) as a white solid; R_f 0.75 (hexane/EtOAc, 4:1); mp 79-80 °C. ^{1}H NMR (500 MHz, $CDCl_3$) δ 3.34 (s, 8H), 2.65−2.58 (m, 2H), 1.45 (s, 36H), 1.14 (d, J = 6.0 Hz, 6H). ^{13}C NMR (126 MHz, $CDCl_3$) δ 171.56, 80.49, 61.92, 53.87, 28.11, 12.69.

The product **37b** was obtained as the by-product. Yield: 4% as a white solid; R_f 0.1 (hexane/EtOAc, 4:1); mp 45−47 °C. ^{1}H NMR (500 MHz, $CDCl_3$) δ 3.52 (d, J = 17.4 Hz, 4H), 3.42 (d, J = 17.4 Hz, 4H), 2.96−2.89 (m, 2H), 1.45 (s, 36H), 1.04 (d, J = 6.7 Hz, 6H). ^{13}C NMR (126 MHz, $CDCl_3$) δ 171.82, 80.47, 59.93, 54.27, 28.12, 12.99.

*meso-2,3-Diaminobutane-N,N,N′,N′-tetraacetic Acid Dihydrochloride (**38a**).* The solution of compound **37a** (4.58 g, 8.41 mmol) and 36% aq. HCl (14.7 mL, 0.166 mol) in H_2O (25 mL) was heated to 85 °C for 3 h. The solvent was evaporated and the resulting product **38** was dried over P_2O_5. Yield: 99% as a white solid. ^{1}H NMR (500 MHz, D_2O) δ 3.95 (d, J = 17.7 Hz, 4H), 3.72 (d, J = 17.7 Hz, 4H), 3.46−3.38 (m, 2H), 1.14 (d, J = 6.5 Hz, 6H). ^{13}C NMR (126 MHz, D_2O) δ 172.86, 62.95, 54.22, 9.77.

*rac-2,3-Diaminobutane-N,N,N′,N′-tetraacetic Acid Dihydrochloride (**38b**).* The solution of compound **37b** (0.85 g, 1.56 mmol) and 36% aq. HCl (2.76 mL, 31.2 mmol) in H_2O (10 mL) was heated to 85 °C for 3 h. The solvent was evaporated and the resulting product **38b** was dried over P_2O_5. Yield: 99% as a white solid. ^{1}H NMR (500 MHz, DMSO) δ 3.81 (d, J = 17.5 Hz, 4H), 3.67 (d, J = 17.6 Hz, 4H), 3.36−3.29 (m, 2H), 1.08 (d, J = 5.4 Hz, 6H). ^{13}C NMR (126 MHz, DMSO) δ 170.18, 60.16, 10.12.

*meso-Tetramethyl 2,3-diaminobutane-N,N,N′,N′-tetraacetate (**39**).* Thionyl chloride (10 g, 6 mL, 0.084 mol) was added dropwise to a suspension of *meso*-2,3-diaminobutane-*N,N,N′,N′*-tetraacetic acid dihydrochloride **38a** (3.28 g, 0.0083 mol) in CH_3OH (100 mL) at 5 °C. The reaction mixture was stirred at rt for 24 h. The volatiles were evaporated under reduced pressure. The residue was partitioned between EtOAc (100 mL) and a saturated solution of $NaHCO_3$ (100 mL). The organic layer was separated, washed with water (2 × 70 mL), dried over anhydrous Na_2SO_4, and evaporated under reduced pressure. Yield: 92% as a white solid; mp 82−84 °C. ^{1}H NMR (500 MHz, $CDCl_3$) δ 3.68 (s, 12H), 3.49 (s, 8H), 2.72−2.64 (m, 2H), 1.13 (d, J = 6.4 Hz, 6H). ^{13}C NMR (126 MHz, $CDCl_3$) δ 172.53, 61.96, 52.60, 51.48, 12.46.

*meso-4,4′-(Butane-2,3-diyl)bis(piperazine-2,6-dione) (**11**).* The solution of compound **39** (2.3 g, 6.11 mmol) and formamide (2.75 g, 2.44 mL, 61.06 mmol) in dioxane (25 mL) was added to the suspension of NaH (60% in mineral oil, 2. g, 72.5 mmol) in dioxane (25 mL) at 10 °C under an argon atmosphere. The reaction mixture was stirred at rt for 24 h. Then, the reaction mixture was mixed with hexane (90 mL), stirred for 20 min, and filtered. The precipitate was carefully dissolved in water with crushed ice (70 mL) and the resulting solution was treated with 36% aq. HCl to pH 4−5. The formed precipitate was filtered and dried to give 0.64 g of the product **11**. The filtrate was partially evaporated under reduced pressure and the formed precipitate was filtered to give an additional 0.27 g of product **11**. Yield: 53% (0.91 g) as a white solid; 55% (8.25 g) when stared from 20.06 g of *meso*-tetramethyl 2,3-diaminobutane-*N,N,N′,N′*-tetraacetate; mp 315−317 °C (with decomp.). ^{1}H NMR (500 MHz, DMSO-d_6) δ 11.01 (s, 2H), 3.32 (dd, J = 16.4, 1.7 Hz, 4H), 3.22 (dd, J = 16.4, 1.6 Hz, 4H), 2.78−2.72 (m, 2H), 0.89 (d, J = 5.9 Hz, 6H). ^{13}C NMR (126 MHz, DMSO-d_6) δ 172.27, 58.86, 51.87, 9.44. Anal. calcd for $C_{12}H_{18}N_4O_4$: C, 51.06; H, 6.43; N, 19.85. Found: C, 50.84; H, 6.12; N, 19.64. HRMS (ESI$^+$) calcd for $(C_{12}H_{18}N_4O_4 + H)^+$ m/z: 283.14008; found: 283.1407.

*rac-4,4′-(Butane-2,3-diyl)bis(piperazine-2,6-dione) (**12**).* Compound **38b** (1.3 g, 3.3 mmol) was mixed with formamide (5 mL), and the reaction mixture was heated under reduced pressure (30 mbar) at 110 °C for 1.5 h. Then, the reaction vessel was filled with argon and the reaction mixture was heated for another 5 h at 150−160 °C under an argon atmosphere. Upon completion, formamide was distilled off under reduced pressure (30 mbar), the residue was

https://doi.org/10.1021/acs.jmedchem.0c02157
J. Med. Chem. 2021, 64, 3997−4019

cooled to rt, and MeOH (5 mL) was added. The resulting suspension was stirred at rt overnight. The crystalline product was filtered, washed with another MeOH (5 mL), and dried. Yield: 20% as a brownish solid; mp 270−272 °C with decomposition. ^{1}H NMR (500 MHz, DMSO-d_6) δ 10.93 (s, 2H), 3.40 (d, J = 16.6 Hz, 4H), 3.32 (d, J = 16.6 Hz, 4H, overlapped with H_2O), 2.85−2.80 (m, 2H), 0.86 (d, J = 6.0 Hz, 6H). ^{13}C NMR (126 MHz, DMSO-d_6) δ 172.25, 57.86, 51.58, 12.36. HRMS (ESI$^+$) calcd for $(C_{12}H_{18}N_4O_4 + H)^+$ m/z: 283.14008; found: 283.1405.

General Method for the Synthesis of Hydrolysis Products 1-hp, 2-hp, 11-hp, and 12-hp. The mixtures of compound **1**, **2**, **11**, or **12** (0.7 mmol) and 1 M NaOH (1.75 mL, 2.5 equiv) in H_2O (4 mL) were stirred at rt for 24 h. The reaction mixtures were acidified with Amberlyst 15 (hydrogen form) to pH 4. Amberlyst 15 was filtered off and the clear aqueous filtrate was evaporated to dryness under reduced pressure. The crude products **1-hp**, **2-hp**, **11-hp**, or **12-hp** were further dried under reduced pressure over P_2O_5 and used without further purification.

1-hp. MS (ESI$^+$): m/z (%) = 323.07 (100) $[M + H]^+$; 345.00 (50) $[M + Na]^+$; MS (ESI$^-$): m/z (%) = 321.2 (45) $[M - H]^-$; 343.20 (100) $[M - 2H + Na]^-$.

2-hp. MS (ESI$^+$): m/z (%) = 278.07 (100) $[M + H]^+$; 300.09 (25) $[M + Na]^+$.

11-hp. MS (ESI$^+$): m/z (%) = 318.93 (100) $[M + H]^+$; 341.07 (15) $[M + Na]^+$.

12-hp. MS (ESI$^+$): m/z (%) = 318.92 (100) $[M + H]^+$; 341.08 (17) $[M + Na]^+$.

Toxicities of Studied Compounds on the Neonatal Rat Cardiomyocytes and Their Ability to Prevent DAU-Induced Cardiotoxicity. The NVCMs were isolated from 1- to 3-day-old Wistar rats. Briefly, the hearts were minced in a buffer (1.2 mM $MgSO_4 \cdot 7H_2O$; 116 mM NaCl; 5.3 mM KCl; 1.13 mM $NaH_2PO_4 \cdot H_2O$; 20 mM 4-(2-hydroxyethyl)-1-piperazine ethanesulfonic acid (HEPES)) on ice, then serially digested (20 min, six repetitions) at 37 °C with collagenase type II (60 U/mL, Gibco). After 2 h preplating on 150 mm Petri dish per approx. 20 hearts to minimize nonmyocyte contamination, the cells were plated on 24-well gelatin-coated plates in a density of 400 000 cells per well. NVCMs were cultured at 37 °C and 5% CO_2 in the Dulbecco's modified Eagle's medium (DMEM)/F12 culture medium supplemented with 10% horse serum, 5% fetal bovine serum (FBS), 20 mM sodium pyruvate, 50 U/mL penicillin, and 50 μg/mL streptomycin. Freshly isolated NVCMs were left for 40 h to attach and form a culture of spontaneously beating cardiomyocytes, then the medium was changed to DMEM/F12 medium supplemented with 5% fetal bovine serum, 20 mM sodium pyruvate, 50 U/mL penicillin, and 50 μg/mL streptomycin. For the experiments, the medium was changed to serum- and pyruvate-free DMEM/F12 with 50 U/mL penicillin and 50 μg/mL streptomycin. In this medium, the cells were maintained to the end of the experiment. The myocytes were pretreated with DEX or the novel analogues for 3 h, and then coincubated with DAU for 3 h or incubated without DAU (own toxicity of compounds). After the DAU treatment period, the culture medium was changed for the drug-free DMEM/F12 with 50 U/mL penicillin and 50 μg/mL streptomycin for the 48 h follow-up. Subsequently, the sample of the culture medium was taken from each well for the assessment of the lactate dehydrogenase (LDH) activity; the control wells were treated with lysis buffer (0.1 M potassium phosphate, 1% Triton X-100, 1 mM dithiothreitol (DTT), 2 mM EDTA, pH 7.8, 15 min in rt) for total LDH. All of the samples were analyzed immediately in Tris−HCl buffer (pH 8.9) containing 35 mM lactic acid and 5 mM NAD^+. The rate of NAD^+ reduction was monitored spectrophotometrically at 340 nm for 2 min. The slope of the linear region was calculated, and the data were expressed as the percent of total LDH.

Assessments of the Antiproliferative Activity. The HL-60 cell line, derived from a single patient with acute promyelocytic leukemia,[65] was purchased from the American Type Culture Collection. The cells were cultured in Roswell Park Memorial Institute (RPMI)-1640 supplemented with 10% fetal bovine serum (FBS), 50 U/mL penicillin and 50 μg/mL streptomycin (all from Lonza, Belgium) in 75 cm^2 tissue culture flasks (TPP, Switzerland) at 37 °C in a humidified atmosphere of 5% CO_2. For the cytotoxicity assays, the cells were plated on 96-well plates (TPP, Switzerland) in a density of 10 000 cells per well (100 000 cells/mL). The cells were incubated with examined agents or their combinations for 72 h. The proliferation was determined using the XTT assay. Briefly, 25 μL of XTT/phenazine methosulfate (PMS) solution in phosphate-buffered saline (PBS) (1 mg/mL 2,3-bis-(2-methoxy-4-nitro-5-sulfophenyl)-2H-tetrazolium-5-carboxanilide (XTT; Serva, Germany), 50 μM phenazine methosulfate (PMS); filtered through 0.22 μm filter) was added to each well, and after 4 h of incubation at 37 °C (5% CO_2) the absorbance was measured at 450 nm.

Inhibition of Human Recombinant Topoisomerase II Isoforms. The TOP2 activity assay was performed using recombinant human TOP2A or TOP2B (Inspiralis, U.K.) incubated with kDNA isolated in house as described previously[66] in a reaction buffer containing 55 mM Tris−HCl (pH 7.5), 135 mM NaCl, 10 mM $MgCl_2$, 5 mM DTT, 0.1 mM EDTA, 3 mM ATP, 100 μg/mL bovine serum albumin, and 1/10 volume of each compound diluted in 10% DMSO (final DMSO concentration 1%) for 30 min at 37 °C. The reaction was then stopped by the addition of gel loading buffer (equal volume; 40% (w/v) sucrose, 10 mM EDTA, 0.5 mg/mL bromophenol blue, 100 mM Tris−HCl (pH 8)), and the samples were analyzed on a 1% agarose gel in TAE buffer (40 mM Tris base, 20 mM acetic acid, 1 mM EDTA, pH 8.3) at 3 V/cm for approximately 2 h. Gels were stained with SYBR Safe (Thermo Fisher Scientific) for 15 min and visualized using a Gel Doc EZ with Image Lab software (Bio-Rad, Hercules, CA). The signal of the treated samples was normalized to the value of the control (untreated sample; 100%) present on the same gel. The normalized signal of three independent measurements was then expressed as mean ± SD.

Western Blot Analysis of Topoisomerase II in Cardiomyocytes. The NVCMs plated on 24-well plates were incubated with DEX or its analogues for 24 h, washed with PBS, and lysed in 75 μL of lysis buffer (2% sodium dodecyl sulfate (SDS) in 50 mM Tris−HCl (pH 6.8), 1 mM EDTA). Total protein in the lysate was assessed by the bicinchoninic acid (BCA) protein assay (Cyanagen, Italy), and 10 μg of protein in sample buffer (0.05% bromophenol blue, 0.1 M DTT, 10% glycerol, 50 mM Tris−HCl (pH 6.8)) was loaded into each lane of 1 mm/15 well 7.5% TGX Mini-PROTEAN Stain-Free gel (Bio-Rad). After the separation (100 V constant, approx. 90 min), the proteins were electrically transferred using Trans-Blot Turbo (Bio-Rad; 10 min, 2.5 A const, approx. 15−20 V) onto a nitrocellulose membrane (Bio-Rad). Rabbit monoclonal anti-TOP2A/B (EPR 3577; Abcam, U.K.; dilution 1:2000) and horseradish peroxidase-conjugated goat anti-rabbit IgG (Goat F(ab′)2 Anti-Rabbit IgG F(ab′)2 (horseradish peroxidase (HRP)) preadsorbed (ab6112), Abcam, U.K.; dilution 1:5000) were used for immunostaining with enhanced chemiluminescence detection (Clarity, Bio-Rad). Densitometric quantification was performed using Image Lab software (Bio-Rad) with normalization to total protein detected using stain-free technology (Bio-Rad). The integrated signal of the treated samples was further normalized to the respective control (untreated sample; 100%) present on the same membrane. The normalized signal of four independent measurements was then expressed as mean ± SD. Precision Plus Protein Standards Kaleidoscope (Bio-Rad) was used as a molecular weight marker.

Molecular Modeling and Dynamic Simulation Studies. Molecular docking was used for binding poses calculations. The three-dimensional (3D) structure ligands were built using Open Babel, v.2.3.2,[67] and optimized using Avogadro, v.1.2.0 using the general AMBER force field (GAFF).[68] They were converted into pdbqt-format using Open Babel, v. 2.3.2. The yeast Top2B structure was gained from the RCSB database (PDB ID: 1QZR, the crystal structure of the ATPase region of *Saccharomyces cerevisiae* topoisomerase II bound to ICRF-187 (dexrazoxane), resolution 1.90 Å) and prepared for docking by the function DockPrep of the software Chimera, v.1.14,[69] and by MGLTools, v.1.5.4.[70] The docking calculation was performed using Vina, v.1.1.2,[71] as semiflexible with a flexible ligand and a rigid receptor.

https://doi.org/10.1021/acs.jmedchem.0c02157
J. Med. Chem. 2021, 64, 3997−4019

The docking poses of DEX, *meso*-**11**, (*R*,*R*)-**12**, and (*S*,*S*)-**12** were improved by the MD simulation. The receptor structure was prepared by the software Chimera. The best-scored docking pose was taken as the initial state for MD. The force-field parameters for ligands were assessed using Antechamber,[72] v.20.0 using GAFF.[73] MD simulations were carried out using Gromacs, v. 2018.1.[74] The complex receptor−ligand was solvated in the periodic water box using the TIP3P model.[75] The system was neutralized by adding Na^+ and Cl^- ions to a concentration of 10 nM. The system energy was minimalized and equilibrated in a 100 ps isothermal-isochoric NVT and then a 100 ps isothermal-isobaric NPT phase. Then, a 10 ns MD simulation was run at a temperature of 300 K. The molecular docking and MD results were 3D visualized using The PyMOL Molecular Graphics System, version 2.0.6, Schrödinger, LLC.

Displacement of Iron Ions from the Complex with DAU. The rates of Fe^{3+} displacement from the DAU-Fe^{3+} complex by DEX and its selected analogues **1**, **2**, and **11** and their degradation products were measured using a modified spectrophotometric assay described previously.[76] A complex of DAU and Fe^{3+} (3:1 in 15 mM HCl) was added to the reaction buffer (50 mM Tris/150 mM KCl, pH = 7.4, rt) in one well of a 96-well microplate to yield a final concentration of 45 μM DAU and 15 μM Fe^{3+}. The absorbance was measured at λ = 600 nm using a Tecan Infinite 200 plate reader. After 3 min of equilibration, the studied substances (or the reference chelators EDTA and SIH, all 100 μM) have been added and the absorbance was measured for further 10 min.

■ ASSOCIATED CONTENT

Supporting Information

The Supporting Information is available free of charge at https://pubs.acs.org/doi/10.1021/acs.jmedchem.0c02157.

Determination of ICRF-193 (**11**) in racemate **12**, copies of NMR and HRMS spectra of all final compounds (Figures S1−S6) (PDF)

PDB file for DEX docking (PDB)

PDB file for compound **10** docking (PDB)

PDB file for compound **11** docking (PDB)

PDB file for compound (*R*,*R*)-**12** docking (PDB)

PDB file for compound (*S*,*S*)-**12** docking (PDB)

Molecular formula strings and associated biological data (CSV) (CSV)

PDB file for DEX MD simulation (PDB)

PDB file for compound *meso*-**11** MD simulation (PDB)

PDB file for compound (*S*,*S*)-**12** MD simulation (PDB)

PDB file for compound (*R*,*R*)-**12** MD simulation (PDB)

■ AUTHOR INFORMATION

Corresponding Authors

Anna Jirkovská − *Faculty of Pharmacy in Hradec Králové, Charles University, 50005 Hradec Králové, Czech Republic*; Email: jirkovan@faf.cuni.cz

Jaroslav Roh − *Faculty of Pharmacy in Hradec Králové, Charles University, 50005 Hradec Králové, Czech Republic*; orcid.org/0000-0003-4698-8379; Email: jaroslav.roh@faf.cuni.cz

Authors

Galina Karabanovich − *Faculty of Pharmacy in Hradec Králové, Charles University, 50005 Hradec Králové, Czech Republic*

Jan Kubeš − *Faculty of Pharmacy in Hradec Králové, Charles University, 50005 Hradec Králové, Czech Republic*

Veronika Skalická − *Faculty of Pharmacy in Hradec Králové, Charles University, 50005 Hradec Králové, Czech Republic*

Iuliia Melnikova − *Faculty of Pharmacy in Hradec Králové, Charles University, 50005 Hradec Králové, Czech Republic*

Jan Korábečný − *Biomedical Research Center, University Hospital Hradec Kralove, 50005 Hradec Králové, Czech Republic; Faculty of Military Health Sciences, University of Defence, 50005 Hradec Králové, Czech Republic*

Tomáš Kučera − *Faculty of Military Health Sciences, University of Defence, 50005 Hradec Králové, Czech Republic*; orcid.org/0000-0001-6650-1738

Eduard Jirkovský − *Faculty of Pharmacy in Hradec Králové, Charles University, 50005 Hradec Králové, Czech Republic*

Lucie Nováková − *Faculty of Pharmacy in Hradec Králové, Charles University, 50005 Hradec Králové, Czech Republic*

Hana Bavlovič Piskáčková − *Faculty of Pharmacy in Hradec Králové, Charles University, 50005 Hradec Králové, Czech Republic*

Josef Škoda − *Faculty of Pharmacy in Hradec Králové, Charles University, 50005 Hradec Králové, Czech Republic*

Martin Štěrba − *Department of Pharmacology, Faculty of Medicine in Hradec Králové, Charles University, 50003 Hradec Králové, Czech Republic*

Caroline A. Austin − *Biosciences Institute, Faculty of Medical Sciences, Newcastle University, Newcastle upon Tyne NE2 4HH, United Kingdom*

Tomáš Šimůnek − *Faculty of Pharmacy in Hradec Králové, Charles University, 50005 Hradec Králové, Czech Republic*

Complete contact information is available at: https://pubs.acs.org/10.1021/acs.jmedchem.0c02157

Notes

The authors declare no competing financial interest.

■ ACKNOWLEDGMENTS

This study was supported by the Czech Science Foundation (GAČR) 18-08169S and 21-16195S and by the project INOMED (no. CZ.02.1.01/0.0/0.0/18_069/0010046) co-funded by the ERDF. J.K., V.S., and J.Š. thank Charles University (projects GAUK 246219, SVV 260 549, and SVV 260 550). J.K. and T.K. acknowledge support by MH CZ-DRO (University Hospital Hradec Kralove, Nr. 00179906) and by long-term development plan (Faculty of Military Health Sciences). The authors would like to thank Prof. Julius Lukeš and Eva Kriegová for the culture of *Crithidia fasciculata*.

■ ABBREVIATIONS

ANT, anthracycline; DAU, daunorubicin; DEX, dexrazoxane; DMSO, dimethyl sulfoxide; DMEM, Dulbecco's modified Eagle's medium; DTT, dithiothreitol; EtOAc, ethyl acetate; HEPES, 4-(2-hydroxyethyl)-1-piperazine ethanesulfonic acid; LDH, lactate dehydrogenase; NVCMs, neonatal rat ventricular cardiomyocytes; PMS, phenazine methosulfate; ROS, reactive oxygen species; SAR, structure−activity relationships; SIH, salicylaldehyde isonicotinoyl hydrazone; THF, tetrahydrofuran; TOP2A, topoisomerase IIα; TOP2B, topoisomerase IIβ; XTT, 2,3-bis-(2-methoxy-4-nitro-5-sulfophenyl)-2*H*-tetrazolium-5-carboxanilide

■ REFERENCES

(1) Creighton, A. M. Bis diketopiperazines. US3,941,790, 1976.

(2) Creighton, A. M.; Hellmann, K.; Whitecross, S. Antitumour activity in a series of bisdiketopiperazines. *Nature* **1969**, *222*, 384−385.

(3) Woodman, R. J.; Cysyk, R. L.; Kline, I.; Gang, M.; Venditti, J. M. Enhancement of effectiveness of daunorubicin (Nsc-82151) or adriamycin (Nsc-123127) against early mouse L1210 leukemia with ICRF-159 (Nsc-129943). *Cancer Chemother. Rep., Part 1* **1975**, *59*, 689−695.
(4) Kline, I. Potentially useful combinations of chemotherapy detected in mouse tumor systems. *Cancer Chemother. Rep., Part 2* **1974**, *4*, 33−43.
(5) Kano, Y.; Narita, T.; Suzuki, K.; Akutsu, M.; Suda, K.; Sakamoto, S.; Miura, Y. The effects of ICRF-154 in combination with other anticancer agents in vitro. *Br. J. Cancer* **1992**, *66*, 281−286.
(6) Tanabe, K.; Ikegami, Y.; Ishida, R.; Andoh, T. Inhibition of topoisomerase II by antitumor agents bis(2,6-dioxopiperazine) derivatives. *Cancer Res.* **1991**, *51*, 4903−4908.
(7) Hasinoff, B. B.; Kuschak, T. I.; Yalowich, J. C.; Creighton, A. M. A QSAR study comparing the cytotoxicity and DNA topoisomerase II inhibitory effects of bisdioxopiperazine analogs of ICRF-187 (dexrazoxane). *Biochem. Pharmacol.* **1995**, *50*, 953−958.
(8) Andoh, T.; Ishida, R. Catalytic inhibitors of DNA topoisomerase II. *Biochim. Biophys. Acta, Gene Struct. Expression* **1998**, *1400*, 155−171.
(9) Roca, J.; Ishida, R.; Berger, J. M.; Andoh, T.; Wang, J. C. Antitumor bisdioxopiperazines inhibit yeast DNA topoisomerase II by trapping the enzyme in the form of a closed protein clamp. *Proc. Natl. Acad. Sci. U.S.A.* **1994**, *91*, 1781−1785.
(10) Wheeler, R. H.; Clauw, D. J.; Natale, R. B.; Ruddon, R. W. The cytokinetic and cytotoxic effects of ICRF-159 and ICRF-187 in vitro and ICRF-187 in human bone marrow in vivo. *Invest. New Drugs* **1983**, *1*, 283−295.
(11) Rogojina, A.; Gajewski, S.; Bahmed, K.; Osheroff, N.; Nitiss, J. L. Topoisomerase II Inhibitors: Chemical Biology. In *DNA Topoisomerases and Cancer*; Pommier, Y., Ed.; Springer New York: New York, NY, 2012; pp 211−243.
(12) Huang, K. C.; Gao, H.; Yamasaki, E. F.; Grabowski, D. R.; Liu, S.; Shen, L. L.; Chan, K. K.; Ganapathi, R.; Snapka, R. M. Topoisomerase II poisoning by ICRF-193. *J. Biol. Chem.* **2001**, *276*, 44488−44494.
(13) Wang, L.; Eastmond, D. A. Catalytic inhibitors of topoisomerase II are DNA-damaging agents: Induction of chromosomal damage by merbarone and ICRF-187. *Environ. Mol. Mutagen.* **2002**, *39*, 348−356.
(14) Classen, S.; Olland, S.; Berger, J. M. Structure of the topoisomerase II ATPase region and its mechanism of inhibition by the chemotherapeutic agent ICRF-187. *Proc. Natl. Acad. Sci. U.S.A.* **2003**, *100*, 10629−10634.
(15) Chang, S.; Hu, T.; Hsieh, T.-s. Analysis of a core domain in drosophila DNA topoisomerase II: Targeting of an antitumor agent ICRF-159. *J. Biol. Chem.* **1998**, *273*, 19822−19828.
(16) Jensen, L. H.; Wessel, I.; Møller, M.; Nitiss, J. L.; Sehested, M.; Jensen, P. B. N-terminal and core-domain random mutations in human topoisomerase IIα conferring bisdioxopiperazine resistance. *FEBS Lett.* **2000**, *480*, 201−207.
(17) Jensen, L. H.; Nitiss, K. C.; Rose, A.; Dong, J. W.; Zhou, J. F.; Hu, T.; Osheroff, N.; Jensen, P. B.; Sehested, M.; Nitiss, J. L. A novel mechanism of cell killing by anti-topoisomerase II bisdioxopiperazines. *J. Biol. Chem.* **2000**, *275*, 2137−2146.
(18) Nakazawa, N.; Mehrotra, R.; Arakawa, O.; Yanagida, M. ICRF-193, an anticancer topoisomerase II inhibitor, induces arched telophase spindles that snap, leading to a ploidy increase in fission yeast. *Genes Cells* **2016**, *21*, 978−993.
(19) Hossain, M. S.; Akimitsu, N.; Takaki, T.; Hirai, H.; Sekimizu, K. ICRF-193, a catalytic inhibitor of DNA topoisomerase II, inhibits re-entry into the cell division cycle from quiescent state in mammalian cells. *Genes Cells* **2002**, *7*, 285−294.
(20) Lu, D.-Y.; Xu, B.; Ding, J. Antitumor effects of two bisdioxopiperazines against two experimental lung cancer models in vivo. *BMC Pharmacol.* **2004**, *4*, No. 32.
(21) Lu, D. Y.; Lu, T. R. Anticancer activities and mechanisms of bisdioxopiperazine compounds probimane and MST-16. *Anticancer Agents Med. Chem.* **2010**, *10*, 78−91.
(22) Repta, A. J.; Baltezor, M. J.; Bansal, P. C. Utilization of an enantiomer as a solution to a pharmaceutical problem - application to solubilization of 1,2-di(4-piperazine-2,6-dione)propane. *J. Pharm. Sci.* **1976**, *65*, 238−242.
(23) Štěrba, M.; Popelova, O.; Vavrova, A.; Jirkovsky, E.; Kovarikova, P.; Gersl, V.; Simunek, T. Oxidative stress, redox signaling, and metal chelation in anthracycline cardiotoxicity and pharmacological cardioprotection. *Antioxid. Redox Signaling* **2013**, *18*, 899−929.
(24) Reichardt, P.; Tabone, M. D.; Mora, J.; Morland, B.; Jones, R. L. Risk-benefit of dexrazoxane for preventing anthracycline-related cardiotoxicity: Re-evaluating the European labeling. *Future Oncol.* **2018**, *14*, 2663−2676.
(25) van Dalen, E. C.; Caron, H. N.; Dickinson, H. O.; Kremer, L. C. Cardioprotective interventions for cancer patients receiving anthracyclines. *Cochrane Database Syst. Rev.* **2011**, No. CD003917.
(26) Dawson, K. M. Studies on the stability and cellular distribution of dioxopiperazines in cultured BHK-21S cells. *Biochem. Pharmacol.* **1975**, *24*, 2249−2253.
(27) Schroeder, P. E.; Hasinoff, B. B. The doxorubicin-cardioprotective drug dexrazoxane undergoes metabolism in the rat to its metal ion-chelating form ADR-925. *Cancer Chemother. Pharmacol.* **2002**, *50*, 509−513.
(28) Jones, R. L. Utility of dexrazoxane for the reduction of anthracycline-induced cardiotoxicity. *Expert Rev. Cardiovasc. Ther.* **2008**, *6*, 1311−1317.
(29) Martin, E.; Thougaard, A. V.; Grauslund, M.; Jensen, P. B.; Bjorkling, F.; Hasinoff, B. B.; Tjørnelund, J.; Sehested, M.; Jensen, L. H. Evaluation of the topoisomerase II-inactive bisdioxopiperazine ICRF-161 as a protectant against doxorubicin-induced cardiomyopathy. *Toxicology* **2009**, *255*, 72−79.
(30) Jirkovská-Vávrová, A.; Roh, J.; Lencova-Popelova, O.; Jirkovsky, E.; Hruskova, K.; Potuckova-Mackova, E.; Jansova, H.; Haskova, P.; Martinkova, P.; Eisner, T.; Kratochvil, M.; Sus, J.; Machacek, M.; Vostatkova-Tichotova, L.; Gersl, V.; Kalinowski, D. S.; Muller, M. T.; Richardson, D. R.; Vavrova, K.; Sterba, M.; Simunek, T. Synthesis and analysis of novel analogues of dexrazoxane and its open-ring hydrolysis product for protection against anthracycline cardiotoxicity in vitro and in vivo. *Toxicol. Res.* **2015**, *4*, 1098−1114.
(31) Vavrova, A.; Jansova, H.; Mackova, E.; Machacek, M.; Haskova, P.; Tichotova, L.; Sterba, M.; Simunek, T. Catalytic inhibitors of topoisomerase II differently modulate the toxicity of anthracyclines in cardiac and cancer cells. *PLoS One* **2013**, *8*, No. e76676.
(32) Bures, J.; Jirkovska, A.; Sestak, V.; Jansova, H.; Karabanovich, G.; Roh, J.; Sterba, M.; Simunek, T.; Kovarikova, P. Investigation of novel dexrazoxane analogue JR-311 shows significant cardioprotective effects through topoisomerase IIbeta but not its iron chelating metabolite. *Toxicology* **2017**, *392*, 1−10.
(33) Jirkovský, E.; Jirkovska, A.; Bures, J.; Chladek, J.; Lencova, O.; Stariat, J.; Pokorna, Z.; Karabanovich, G.; Roh, J.; Brazdova, P.; Simunek, T.; Kovarikova, P.; Sterba, M. Pharmacokinetics of the cardioprotective drug dexrazoxane and its active metabolite ADR-925 with focus on cardiomyocytes and the heart. *J. Pharmacol. Exp. Ther.* **2018**, *364*, 433−446.
(34) Atwal, M.; Swan, R. L.; Rowe, C.; Lee, K. C.; Lee, D. C.; Armstrong, L.; Cowell, I. G.; Austin, C. A. Intercalating TOP2 poisons attenuate topoisomerase action at higher concentrations. *Mol. Pharmacol.* **2019**, *96*, 475−484.
(35) Capranico, G.; Tinelli, S.; Austin, C. A.; Fisher, M. L.; Zunino, F. Different patterns of gene expression of topoisomerase II isoforms in differentiated tissues during murine development. *Biochim. Biophys. Acta, Gene Struct. Expression* **1992**, *1132*, 43−48.
(36) Zhang, S.; Liu, X.; Bawa-Khalfe, T.; Lu, L. S.; Lyu, Y. L.; Liu, L. F.; Yeh, E. T. Identification of the molecular basis of doxorubicin-induced cardiotoxicity. *Nat. Med.* **2012**, *18*, 1639−1642.

https://doi.org/10.1021/acs.jmedchem.0c02157
J. Med. Chem. 2021, 64, 3997−4019

(37) Herman, E. H.; Zhang, J.; Hasinoff, B. B.; Chadwick, D. P.; Clark, J. R.; Ferrans, V. J. Comparison of the protective effects against chronic doxorubicin cardiotoxicity and the rates of iron(III) displacement reactions of ICRF-187 and other bisdiketopiperazines. *Cancer Chemother. Pharmacol.* **1997**, *40*, 400−408.
(38) Herman, E. H.; Ferrans, V. J.; Bhat, H. B.; Witiak, D. T. Reduction of chronic doxorubicin cardiotoxicity in beagle dogs by bismorpholinomethyl derivative of razoxane (ICRF-159). *Cancer Chemother. Pharmacol.* **1987**, *19*, 277−281.
(39) Kollárová-Brázdová, P.; Jirkovská, A.; Karabanovich, G.; Pokorná, Z.; Bavlovič Piskáčková, H.; Jirkovský, E.; Kubeš, J.; Lenčová-Popelová, O.; Mazurová, Y.; Adamcová, M.; Skalická, V.; Štěrbová-Kovaříková, P.; Roh, J.; Šimůnek, T.; Štěrba, M. Investigation of structure-activity relationships of dexrazoxane analogues reveals topoisomerase IIβ interaction as a prerequisite for effective protection against anthracycline cardiotoxicity. *J. Pharmacol. Exp. Ther.* **2020**, *373*, 402−415.
(40) Zhang, J.; Herman, E. H.; Ferrans, V. J. Effects of ICRF-186 [(l)1,2-bis(3,5-dioxopiperazinyl-1-yl)propane] on the toxicity of doxorubicin in spontaneously hypertensive rats. *Toxicology* **1994**, *92*, 179−192.
(41) Johnson, H. E.; Crosby, D. G. Reaction of hydantoin with acetals. *J. Org. Chem.* **1962**, *27*, 2077−2080.
(42) Henrick, K.; McPartlin, M.; Munjoma, S.; Owston, P. G.; Peters, R.; Sangokoya, S. A.; Tasker, P. A. An improved synthesis of 1,2,3-triaminopropane - X-ray structure of S-fac-bis(1,2,3-triaminopropane)cobalt(III) chloride. *J. Chem. Soc., Dalton Trans.* **1982**, 225−227.
(43) Novak, V.; Lucansky, J.; Svicekova, M.; Majer, J. New complexanes .32. Preparation and properties of 2-methyl-1,2-diaminopropane-N,N,N′,N′-tetraacetic acid. *Chem. Zvesti* **1978**, *32*, 19−26.
(44) Snapka, R. M.; Woo, S. H.; Blokhin, A. V.; Witiak, D. T. Inhibition of topoisomerase II by ICRF-193, the meso isomer of 2,3-bis(2,6-dioxopiperazin-4-yl)butane - Critical dependence on 2,3-butanediyl linker absolute configuration. *Biochem. Pharmacol.* **1996**, *52*, 543−549.
(45) Hasinoff, B. B.; Schroeder, P. E.; Patel, D. The metabolites of the cardioprotective drug dexrazoxane do not protect myocytes from doxorubicin-induced cytotoxicity. *Mol. Pharmacol.* **2003**, *64*, 670−678.
(46) Chou, T. C. Drug combination studies and their synergy quantification using the Chou-Talalay method. *Cancer Res.* **2010**, *70*, 440−446.
(47) Downes, C. S.; Clarke, D. J.; Mullinger, A. M.; Giménez-Abián, J. F.; Creighton, A. M.; Johnson, R. T. A topoisomerase II-dependent G2 cycle checkpoint in mammalian cells. *Nature* **1994**, *372*, 467−470.
(48) Clarke, D. J.; Vas, A. C.; Andrews, C. A.; Díaz-Martínez, L. A.; Gimenez-Abian, J. F. Topoisomerase II checkpoints: Universal mechanisms that regulate mitosis. *Cell Cycle* **2006**, *5*, 1925−1928.
(49) Lyu, Y. L.; Kerrigan, J. E.; Lin, C. P.; Azarova, A. M.; Tsai, Y. C.; Ban, Y.; Liu, L. F. Topoisomerase IIbeta mediated DNA double-strand breaks: implications in doxorubicin cardiotoxicity and prevention by dexrazoxane. *Cancer Res.* **2007**, *67*, 8839−8846.
(50) Deng, S.; Yan, T.; Jendrny, C.; Nemecek, A.; Vincetic, M.; Godtel-Armbrust, U.; Wojnowski, L. Dexrazoxane may prevent doxorubicin-induced DNA damage via depleting both topoisomerase II isoforms. *BMC Cancer* **2014**, *14*, No. 842.
(51) Isik, S.; Sano, K.; Tsutsui, K.; Seki, M.; Enomoto, T.; Saitoh, H.; Tsutsui, K. The SUMO pathway is required for selective degradation of DNA topoisomerase IIβ induced by a catalytic inhibitor ICRF-193. *FEBS Lett.* **2003**, *546*, 374−378.
(52) Hasinoff, B. B.; Patel, D.; Wu, X. A QSAR study that compares the ability of bisdioxopiperazine analogs of the doxorubicin cardioprotective agent dexrazoxane (ICRF-187) to protect myocytes with DNA topoisomerase II inhibition. *Toxicol. Appl. Pharmacol.* **2020**, *399*, No. 115038.
(53) Velázquez-Libera, J. L.; Durán-Verdugo, F.; Valdés-Jiménez, A.; Núñez-Vivanco, G.; Caballero, J. LigRMSD: a web server for automatic structure matching and RMSD calculations among identical and similar compounds in protein-ligand docking. *Bioinformatics* **2020**, *36*, 2912−2914.
(54) Hellmann, K.; Rhomberg, W. Dexrazoxane. In *Razoxane and Dexrazoxane—Two Multifunctional Agents: Experimental and Clinical Results*; Hellmann, K.; Rhomberg, W., Eds.; Springer: Netherlands, 2011; pp 157−235.
(55) Hasinoff, B. B. The interaction of the cardioprotective agent ICRF-187 ((+)-1,2-bis(3,5-dioxopiperazinyl-1-yl)propane) - its hydrolysis product (ICRF-198) - and other chelating-agents with the Fe(III) and Cu(II) complexes of adriamycin. *Agents Actions* **1989**, *26*, 378−385.
(56) Hasinoff, B. B. Self-reduction of the iron(III)-doxorubicin complex. *Free Radicals Biol. Med.* **1989**, *7*, 583−593.
(57) Davies, K. J.; Doroshow, J. H.; Hochstein, P. Mitochondrial NADH dehydrogenase-catalyzed oxygen radical production by adriamycin, and the relative inactivity of 5-iminodaunorubicin. *FEBS Lett.* **1983**, *153*, 227−230.
(58) Doroshow, J. H. Anthracycline antibiotic-stimulated superoxide, hydrogen peroxide, and hydroxyl radical production by NADH dehydrogenase. *Cancer Res.* **1983**, *43*, 4543−4551.
(59) Huang, Z. X.; May, P. M.; Quinlan, K. M.; Williams, D. R.; Creighton, A. M. Metal binding by pharmaceuticals. Part 2. Interactions of Ca(II), Cu(II), Fe(II), Mg(II), Mn(II) and Zn(II) with the intracellular hydrolysis products of the antitumour agent ICRF-159 and its inactive homologue ICRF-192. *Agents Actions* **1982**, *12*, 536−542.
(60) Ishida, R.; Iwai, M.; Hara, A.; Andoh, T. The combination of different types of antitumor topoisomerase II inhibitors, ICRF-193 and VP-16, has synergistic and antagonistic effects on cell survival, depending on treatment schedule. *Anticancer Res.* **1996**, *16*, 2735−2740.
(61) Šimůnek, T.; Sterba, M.; Popelova, O.; Adamcova, M.; Hrdina, R.; Gersl, V. Anthracycline-induced cardiotoxicity: Overview of studies examining the roles of oxidative stress and free cellular iron. *Pharmacol. Rep.* **2009**, *61*, 154−171.
(62) Lovejoy, D. B.; Richardson, D. R. Iron chelators as antineoplastic agents: Current developments and promise of the PIH class of chelators. *Curr. Med. Chem.* **2003**, *10*, 1035−1049.
(63) Lenčo, J.; Lenčová-Popelová, O.; Link, M.; Jirkovská, A.; Tambor, V.; Potůčková, E.; Stulík, J.; Šimůnek, T.; Štěrba, M. Proteomic investigation of embryonic rat heart-derived H9c2 cell line sheds new light on the molecular phenotype of the popular cell model. *Exp. Cell Res.* **2015**, *339*, 174−186.
(64) Herman, E. H.; el-Hage, A. N.; Creighton, A. M.; Witiak, D. T.; Ferrans, V. J. Comparison of the protective effect of ICRF-187 and structurally related analogues against acute daunorubicin toxicity in Syrian golden hamsters. *Res. Commun. Chem. Pathol. Pharmacol.* **1985**, *48*, 39−55.
(65) Collins, S. J. The HL-60 promyelocytic leukemia cell line: proliferation, differentiation, and cellular oncogene expression. *Blood* **1987**, *70*, 1233−1244.
(66) Shapiro, T. A.; Klein, V. A.; Englund, P. T. Isolation of Kinetoplast DNA. In *DNA Topoisomerase Protocols: Volume I: DNA Topology and Enzymes*; Bjornsti, M.-A.; Osheroff, N., Eds.; Humana Press: Totowa, NJ, 1999; pp 61−67.
(67) O'Boyle, N. M.; Banck, M.; James, C. A.; Morley, C.; Vandermeersch, T.; Hutchison, G. R. Open Babel: An open chemical toolbox. *J. Cheminf.* **2011**, *3*, No. 33.
(68) Hanwell, M. D.; Curtis, D. E.; Lonie, D. C.; Vandermeersch, T.; Zurek, E.; Hutchison, G. R. Avogadro: an advanced semantic chemical editor, visualization, and analysis platform. *J. Cheminf.* **2012**, *4*, No. 17.
(69) Pettersen, E. F.; Goddard, T. D.; Huang, C. C.; Couch, G. S.; Greenblatt, D. M.; Meng, E. C.; Ferrin, T. E. UCSF Chimera - a visualization system for exploratory research and analysis. *J. Comput. Chem.* **2004**, *25*, 1605−1612.
(70) Morris, G. M.; Huey, R.; Lindstrom, W.; Sanner, M. F.; Belew, R. K.; Goodsell, D. S.; Olson, A. J. AutoDock4 and AutoDockTools4:

https://doi.org/10.1021/acs.jmedchem.0c02157
J. Med. Chem. 2021, 64, 3997−4019

automated docking with selective receptor flexibility. *J. Comput. Chem.* **2009**, *30*, 2785−2791.
(71) Trott, O.; Olson, A. J. AutoDock Vina: Improving the speed and accuracy of docking with a new scoring function, efficient optimization, and multithreading. *J. Comput. Chem.* **2010**, *31*, 455−461.
(72) Wang, J.; Wang, W.; Kollman, P. A.; Case, D. A. Automatic atom type and bond type perception in molecular mechanical calculations. *J. Mol. Graphics Modell.* **2006**, *25*, 247−260.
(73) Wang, J.; Wolf, R. M.; Caldwell, J. W.; Kollman, P. A.; Case, D. A. Development and testing of a general amber force field. *J. Comput. Chem.* **2004**, *25*, 1157−1174.
(74) Abraham, M. J.; Murtola, T.; Schulz, R.; Páll, S.; Smith, J. C.; Hess, B.; Lindahl, E. GROMACS: High performance molecular simulations through multi-level parallelism from laptops to supercomputers. *SoftwareX* **2015**, *1*−*2*, 19−25.
(75) Mark, P.; Nilsson, L. Structure and dynamics of the TIP3P, SPC, and SPC/E water models at 298 K. *J. Phys. Chem. A* **2001**, *105*, 9954−9960.
(76) Buss, J. L.; Hasinoff, B. B. The one-ring open hydrolysis product intermediates of the cardioprotective agent ICRF-187 (dexrazoxane) displace iron from iron-anthracycline complexes. *Agents Actions* **1993**, *40*, 86−95.

https://doi.org/10.1021/acs.jmedchem.0c02157
J. Med. Chem. 2021, 64, 3997−4019